Geophys. J. Int. (2003) **154,** 8–34

An integrated global model of present-day plate motions and plate boundary deformation

Corné Kreemer,[1,*] William E. Holt[1] and A. John Haines[2]

[1] *Department of Geosciences, State University of New York, Stony Brook,* NY 11794-2100, *USA. E-mail: kreemer@geologie.ens.fr*
[2] *Bullard Laboratories, Cambridge University, Cambridge* CB3 0EZ

Accepted 2002 December 11. Received 2002 November 22; in original form 2001 July 9

SUMMARY

In this paper we present a global model (GSRM-1) of both horizontal velocities on the Earth's surface and horizontal strain rates for almost all deforming plate boundary zones. A model strain rate field is obtained jointly with a global velocity field in the process of solving for a global velocity gradient tensor field. In our model we perform a least-squares fit between model velocities and observed geodetic velocities, as well as between model strain rates and observed geological strain rates. Model velocities and strain rates are interpolated over a spherical Earth using bi-cubic Bessel splines. We include 3000 geodetic velocities from 50 different, mostly published, studies. Geological strain rates are obtained for central Asia only and they are inferred from Quaternary fault slip rates. For all areas where no geological information is included *a priori* constraints are placed on the style and direction (but not magnitude) of the model strain rate field. These constraints are taken from a seismic strain rate field inferred from (normalized) focal mechanisms of shallow earthquakes. We present a global solution of the second invariant of the model strain rate field as well as strain rate solutions for a few selected plate boundary zones. Generally, the strain rate tensor field is consistent with geological and seismological data. With the assumption of plate rigidity for all areas other than the plate boundary zones we also present relative angular velocities for most plate pairs. We find that in general there is a good agreement between the present-day plate motions we obtain and long-term plate motions, but a few significant differences exist. The rotation rates for the Indian, Arabian and Nubian plates relative to Eurasia are 30, 13 and 50 per cent slower than the NUVEL-1A estimate, respectively, and the rotation rate for the Nazca Plate relative to South America is 17 per cent slower. On the other hand, Caribbean–North America motion is 76 per cent faster than the NUVEL-1A estimate. While crustal blocks in the India–Eurasia collision zone move significantly and self-consistently with respect to bounding plates, only a very small motion is predicted between the Nubian and Somalian plates. By integrating plate boundary zone deformation with the traditional modelling of angular velocities of rigid plates we have obtained a model that has already been proven valuable in, for instance, redefining a no-net-rotation model of surface motions and by confirming a global correlation between seismicity rates and tectonic moment rates along subduction zones and within zones of continental deformation.

Key words: continental tectonics, global, GPS, plate boundary, plate motions.

1 INTRODUCTION

Plate tectonics has established itself as the most fundamental conceptual model in modern-day geology and geophysics by explaining most first-order geophysical observations on Earth in a comprehensive and self-consistent manner (e.g. Vine & Matthews 1963; Isacks *et al.* 1968; Dewey & Bird 1970; Sclater & Franchateau 1970). Although successful as a theory, the concept of plate tectonics is built on the approximate assumption that plates are rigid and plate boundaries are narrow. Both assumptions are only partially correct (e.g. Gordon 1998). Plate boundaries are narrow (∼1–60 km) along the majority of oceanic ridges and transforms, but they appear much wider within most continental boundary zones and within some oceanic areas. The combined oceanic and continental diffuse plate boundary zones cover ∼15 per cent of the Earth's surface (Gordon & Stein 1992). Only recently, with the vast increase in geodetic observations of crustal motions, has it become possible to measure relative (horizontal) velocities and quantify crustal deformation within (diffuse) plate boundary zones with high accuracy (e.g.

*Now at: Collège de France and Laboratoire de Geologie, Ecole normale supérieure, Paris, France.

Stein 1993). As a result, our understanding of the behaviour of plate boundary zones has increased significantly and enables us, for example, to begin to distinguish between 'block-like' (e.g. Tapponnier *et al.* 1982; Avouac & Tapponnier 1993; Peltzer & Saucier 1996) versus continuous deformation (e.g. England & McKenzie 1982; England & Houseman 1986; Molnar 1988). Ultimately, inferences on the fundamental distribution of plate boundary deformation as well as the quantification of strain rates and rotation rates (around a vertical axis) within the crust and lithosphere will allow us to improve upon our understanding of the dynamics that govern plate boundary deformation (e.g. Lamb 1994; Thatcher 1995; Jackson 2002). Furthermore, a complete quantification of the velocity gradient tensor field within plate boundary zones will be of great interest in seismic hazard studies (e.g. Ward 1994; Giardini 1999) and will, most likely, become an integrated part in future plate tectonic and plate motion models.

In this paper we present results of a global velocity gradient tensor field model associated with the accommodation of present-day crustal motions. We refer to this model as the global strain rate model, or GSRM-1. Because we solve for the velocity gradient field over almost the entire surface of the Earth, this is the first study to include plate boundary zones into one global model quantifying the complete present-day surface kinematics. Other global kinematic models that have recognized the importance of estimating the kinematics of plates and plate boundaries simultaneously (Drewes & Angermann 2001) are still limited by a relatively small number of geodetic velocities. Our model combines space geodetic data (i.e. global positioning system (GPS), very long baseline interferometry (VLBI) and Doppler orbitography and radiopositioning integrated by satellite (DORIS)) measured on rigid plates as well as within plate boundary zones. Some regional Quaternary fault slip rate data and seismic moment tensor information from shallow earthquakes are included as well. We show strain rate field solutions for several plate boundary zones and, using the assumption of plate rigidity for plates and blocks far away from known deformation zones, give present-day angular velocities for most plate pairs. We also present a new no-net-rotation model, which is a slight revision of the model recently presented by Kreemer & Holt (2001).

2 METHODOLOGY

The methodology adopted to estimate a global strain rate and velocity model has been presented in Kreemer *et al.* (2000a), but a brief overview is given here. We make the assumption that the lithosphere in plate boundary zones behaves as a continuum. This is a reasonable approximation when considering large-scale deformation for areas that have horizontal dimensions several times the thickness of the brittle elastic layer (e.g. England & McKenzie 1982). We adopt the methodology of Haines & Holt (1993) to estimate the horizontal velocity gradient tensor field on a sphere. A bi-cubic Bessel interpolation is used instead of polynomials, however, to expand a model rotation vector function that is obtained by a least-squares minimization between model and geodetic velocities, and model and geological strain rates (Holt & Haines 1995). Geological strain rates are obtained through a summation of Quaternary fault slip rates using a variant of Kostrov's (1974) formula (Shen-Tu *et al.* 1999; Holt *et al.* 2000a). This type of modelling has been presented in numerous papers concerning regional tectonics in zones of diffuse deformation; e.g. western United States (Shen-Tu *et al.* 1999) and central Asia (Holt *et al.* 2000a). A comprehensive overview of the methodology can be found in Haines *et al.* (1998), Holt *et al.* (2000b) and Beavan & Haines (2001).

Our model grid is continuous in longitudinal direction and covers the globe between 80°N and 80°S. Each grid area is $0.6^\circ \times 0.5^\circ$ in dimension. Whether an area is considered to be deforming or not is based primarily on seismicity occurrence (Engdahl *et al.* 1998) and the Harvard Centroid Moment Tensor (CMT) catalogue (Dziewonski *et al.* 1981; Dziewonski *et al.* 2000). All oceanic ridge and transform zones are allowed to deform. Within oceanic and continental regions of diffuse deformation, where seismicity rates are often low, the designation of boundaries between deforming and plate-like regions was often subjective. Therefore, the geometry of deforming regions in this model should be viewed as being approximate. About 24 500 grid areas cover the Earth's deforming regions; all other areas are considered to be rigid. The rigid areas mimic 25 independent plates and blocks, including a number of relatively small entities such as the Rivera, Anatolian, Okhotsk, Caroline, Scotia, Sunda, Tarim, Amurian and South China plates and blocks, among others.

To accommodate the fact that not all plate boundary zones or areas within one single plate boundary zone strain with the same magnitude we constrain the magnitude of the *a priori* strain rate variance to vary globally. In order to do this all plate boundary zones are divided into 218 smaller areas. For each of these areas a value is assigned, depending on the expected magnitude of the strain rate for the area. For conformity the strain rate variance is chosen from a range of four values, depending on the expected strain rate (mainly based on seismicity occurrence); the highest *a priori* variance value is reserved for the zones that are expected to deform with the highest strain rate. Following this procedure we maintain some control on the distribution of expected strain rates; i.e. by absence of geodetic velocities and Quaternary fault slip rates that could provide constraints on the strain rate distribution, we can constrain some areas to deform at a higher rate than others. The *a priori* assignment of a heterogeneous strain rate variance distribution is therefore particularly important in obtaining strain rate distributions for areas such as Iran, East African Rift Valley, western Mediterranean, and central America that are consistent with the regional seismicity distribution.

For regions that are not densely sampled with geodetic observations, the interpolation of geodetic velocities can be highly nonunique in describing the regional strain rate field (Kreemer *et al.* 2000b; Beavan & Haines 2001). However, the design of the strain rate covariance matrix can place *a priori* constraints on the style and direction of the model strain rate field. The constraint on the direction of the principal axes of the model strain rate field involves an uncertainty of $\pm 10^\circ$. Information concerning the style and direction of expected strain rate is inferred from the principal axes of the seismic strain rate field, which is obtained through a Kostrov (1974) summation of seismic moment tensors in each grid area. Seismic moment tensors are used only from shallow events ($\leq$40 km) in the Harvard CMT catalogue (1977 January–2000 December). For this purpose all events are weighted equally in the Kostrov summation. This approach is adopted here, except for areas where Quaternary fault slip rate data are used to infer geological strain rate estimates (currently only for central Asia). It should be noted that only the style and direction of the model strain rate field is constrained using the direction and style of the seismic strain rate field, not the magnitude. Also, constraints on the style and direction of the model strain rate field do not significantly affect the fit of the model velocities to the observed velocities. Moreover, including constraints on the style and direction of the model strain rate field results in a solution that is as consistent as possible with regional seismotectonics, while providing more stability in the model strain rate field from one

grid area to another (Kreemer *et al.* 2000b). More specifics on this methodology can be found in Kreemer *et al.* (2000a) and Haines *et al.* (1998).

One of the main advantages of the methodology used for this model is that an unlimited number of geodetic studies may be combined. The original reference frame of each individual study does not need to be adopted and, in fact, can be left undefined, *a priori*, in the inversion; the reference frame is solved upon fitting geodetic velocities to one self-consistent velocity gradient tensor field. That is, implicit in our procedure is the assumption that a single rigid-body rotation can be applied to velocity vectors from each individual study (one rotation vector for each study) such that the model velocity field provides a 'best fit' to the observed vectors that have been rotated into a single model frame of reference. We acknowledge that the assumption that the reference frames of various studies differ only by a single rigid-body rotation is an oversimplification. In addition to the rigid-body rotation there could be a corresponding translation to describe the reference frame difference (formally there is an additional seventh parameter to describe the reference frame difference, but this scaling parameter can be ignored here because we only use horizontal velocities). For small-scale networks this translation vector will be analogous in effect to a rigid-body rotation, and can be ignored. However, our approach to ignore the translational correction may lead to the possibility that we cannot satisfactory resolve the reference frame differences between large-scale networks. Except for one case (described in the next session), we do not observe significant residuals between velocities at colocated sites for larger networks after we have applied the rigid-body rotation. However, we do acknowledge that future modelling may need to incorporate the translational difference as well.

3 DATA

In this study we perform a least-squares fit to 3000 geodetic velocities from 50 different studies. Site locations are shown in Fig. 1 and references are given in Table 1. The majority of the geodetic data consist of GPS velocities. As part of the GPS velocities we include the GPSVEL (version 0.2) model (Lavallée *et al.* 2001). GPSVEL is a global velocity solution determined for 175 global sites that are coordinated by the International GPS Service (IGS) as part of the IGS Densification Project (Zumberge & Liu 1995). The GPSVEL solution is obtained by a rigorous combination of weekly station coordinate estimates from seven global analysis centres and three regional associate analysis centres (Europe, Australia and South America) using a free-network approach (Davies & Blewitt 2000). Only stations with a time-series of at least 4.5 yr are analysed and the methodology of Zhang *et al.* (1997) is used for error analysis. Geodetic velocities that are part of this solution will be referred to as GPSVEL velocities in the remainder of the paper. We also include the VLBI global velocity data set (Ma & Ryan 1998) as well as a subset of the global velocity solution obtained from the DORIS system (Crétaux *et al.* 1998). We found a consistent global misfit between the DORIS velocities and the velocities obtained by VLBI and GPS. This discrepancy could be caused by the fact that we only applied a rigid-body rotation and not a translation to transform the DORIS velocities from their original reference frame into the model reference frame. We tested this possibility by inverting for both the rotation and translation vector using nine colocated sites of the DORIS and GPSVEL networks. We found indeed a significant translation vector. However, although the misfit between DORIS and GPSVEL became much smaller after we applied the obtained rotation and translation vectors to the DORIS reference frame, a significant misfit between DORIS and GPSVEL velocities was still present, which hints at an additional source behind the reference frame discrepancy. Therefore, for now, we have only included DORIS velocities measured at the Nubian (four sites) and Somalian Plate (one site) and at the Djibouti site location. We observe a good consistency between the DORIS velocities and other geodetic velocities when only this subset of the DORIS global data set is used. Most of the studies used in the model are published, but the most current data from

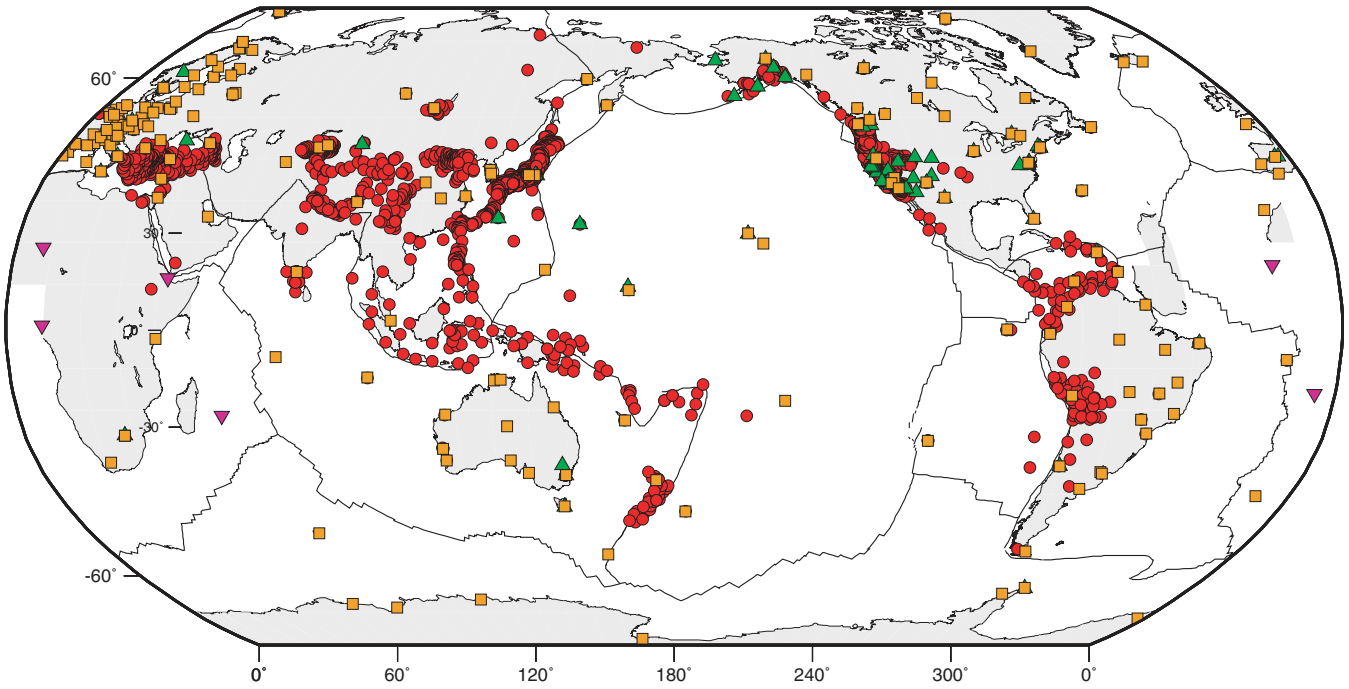

Figure 1. Site locations for which geodetic velocities are used. Circles are regional data (mainly campaign style), squares are stations included in the GPSVEL solution, triangles are VLBI stations and upside-down triangles are DORIS stations.

Table 1. Rotation vectors that rotate geodetic studies from their original reference frame into a model Pacific reference frame.

Source	Region	Sites[a]	σ[b]	Frame[c]	Lat. (°N)	Long. (°E)	$\dot{\omega}$ (°Myr^{-1})	ω_x	ω_y	ω_z	$\rho\,(x, y)$	$\rho\,(x, z)$	$\rho\,(y, z)$
Abdrakhmatov *et al.* (1996)	Tien Shan	79	2	Local	51.6	−88.2	0.89	0.018 ± 0.017	−0.549 ± 0.059	0.694 ± 0.057	0.95	0.94	0.99
Angermann *et al.* (1999)	Nazca Plate	6	1	S. America	58.7	−88.0	0.67	0.012 ± 0.009	−0.349 ± 0.010	0.575 ± 0.009	−0.51	−0.26	0.27
Antonelis *et al.* (1999)	Gulf California	4	1	Local	57.7	−59.9	0.60	0.161 ± 0.563	−0.277 ± 1.901	0.506 ± 0.856	1.00	−1.00	−1.00
Beavan & Haines (2001)	New Zealand	31	2	ITRF96	60.6	−53.0	0.79	0.235 ± 0.050	−0.311 ± 0.008	0.691 ± 0.042	−0.68	0.98	−0.69
Beavan *et al.* (2001)	Luzon (Phil.)	18	1	ITRF96	60.2	−71.2	0.68	0.109 ± 0.009	−0.319 ± 0.011	0.589 ± 0.009	−0.62	0.61	−0.77
Bennett *et al.* (1999)	Basin & Range	46	3	N. America	49.9	−78.5	0.78	0.099 ± 0.006	−0.490 ± 0.011	0.594 ± 0.010	0.78	−0.72	−0.88
Bendick *et al.* (2000)	Altyn Tagh Flt.	15	1	Local	65.4	−63.9	1.19	0.217 ± 0.007	−0.444 ± 0.063	1.080 ± 0.053	−0.06	−0.07	0.98
Bevis *et al.* (1995)	Tonga—Fiji	8	1	Pacific	−74.6	−69.7	0.05	0.004 ± 0.454	−0.012 ± 0.102	−0.046 ± 0.136	0.82	0.91	0.74
Bevis *et al.* (1999)	Central Andes	24	3	S. America	60.3	−89.2	0.68	0.004 ± 0.008	−0.339 ± 0.010	0.595 ± 0.008	−0.51	−0.44	0.47
Calais *et al.* (1998)	Baikal	16	3	ITRF97	65.2	−74.2	0.67	0.077 ± 0.005	−0.270 ± 0.004	0.607 ± 0.007	0.39	0.19	0.10
Chen *et al.* (2000)	Eastern China	57	1	ITRF96	63.8	−76.7	0.65	0.066 ± 0.005	−0.278 ± 0.004	0.581 ± 0.006	0.36	0.14	0.04
Clarke *et al.* (1998)	Corinth Rift	52	1	Eurasia	55.5	−102.3	0.89	−0.107 ± 0.289	−0.492 ± 0.127	0.732 ± 0.252	1.00	1.00	1.00
Cocard *et al.* (1999)	Greece	36	2	Eurasia	66.3	−62.7	1.03	0.189 ± 0.071	−0.366 ± 0.028	0.939 ± 0.061	0.97	0.99	0.97
Crétaux *et al.* (1998)	Nubia–Somalia	6	2	KRF	71.4	−70.0	0.70	0.077 ± 0.023	−0.211 ± 0.009	0.666 ± 0.013	0.08	0.35	−0.14
Dixon *et al.* (1998)	N. Caribbean	4	1	Local	76.5	147.7	0.39	−0.077 ± 0.692	0.048 ± 2.028	0.377 ± 0.841	−1.00	1.00	−1.00
Dixon *et al.* (2000)	Sierra Nevada	12	1	ITRF96	37.1	−107.6	1.23	−0.298 ± 0.080	−0.936 ± 0.135	0.744 ± 0.122	1.00	−1.00	−1.00
Freymueller *et al.* (1999)	N. California	52	1	Pacific	38.9	−125.8	0.67	−0.306 ± 0.122	−0.424 ± 0.195	0.423 ± 0.186	1.00	−1.00	−1.00
Gan *et al.* (2000)	E. California	43	2	ITRF97	52.7	−67.5	0.66	0.153 ± 0.100	−0.369 ± 0.195	0.524 ± 0.161	1.00	−1.00	−1.00
GPSVEL v.0.2	World	175	1	ITRF2000	64.4	−73.4	0.67	0.083 ± 0.004	−0.279 ± 0.003	0.609 ± 0.004	0.43	−0.23	−0.26
Heki *et al.* (1999)	Northeast Asia	10	3	Eurasia	64.6	−83.8	0.87	0.040 ± 0.021	−0.370 ± 0.027	0.783 ± 0.030	−0.83	−0.82	0.86
Jansma *et al.* (2000)	Puerto Rico	7	1	ITRF96	77.1	−80.6	0.57	0.021 ± 0.334	−0.126 ± 0.713	0.560 ± 0.257	−1.00	1.00	−1.00
Kato *et al.* (1998)	W. Pacific	13	2	Local	59.3	−77.8	0.83	0.089 ± 0.017	−0.412 ± 0.012	0.712 ± 0.013	−0.81	−0.68	0.58
Kogan *et al.* (2000)	EU—NA	9	1	N. America	50.5	−78.7	0.74	0.092 ± 0.005	−0.463 ± 0.006	0.573 ± 0.007	0.19	−0.13	−0.45
Kotzev *et al.* (2001)	Bulgaria	17	1	Eurasia	62.3	−84.7	0.90	0.039 ± 0.122	−0.419 ± 0.057	0.801 ± 0.127	1.00	1.00	0.99
Larson *et al.* (1999)	Himalayas	25	1	ITRF94	62.3	−87.6	0.67	0.013 ± 0.009	−0.309 ± 0.048	0.590 ± 0.024	0.62	0.56	0.94
Ma & Ryan (1998)	World	72	td[d]	ITRF96	64.2	−72.3	0.69	0.091 ± 0.004	−0.284 ± 0.003	0.617 ± 0.004	0.44	−0.27	−0.29
McCaffrey *et al.* (2000)	Oregon	50	3	N. America	47.8	−58.3	0.59	0.208 ± 0.082	−0.337 ± 0.126	0.437 ± 0.142	1.00	−1.00	−1.00
McClusky *et al.* (2000)	Greece–Turkey	195	1	Eurasia	62.1	−85.4	0.91	0.034 ± 0.009	−0.425 ± 0.006	0.806 ± 0.010	0.71	0.72	0.57
Michel *et al.* (2001)	Southeast Asia	44	1	ITRF97	63.6	−71.4	0.68	0.096 ± 0.006	−0.285 ± 0.006	0.607 ± 0.006	−0.01	0.05	−0.18
Miller *et al.* (2001)	Pac. Northwest	19	2	N. America	50.9	−77.7	0.78	0.104 ± 0.006	−0.479 ± 0.008	0.604 ± 0.010	0.53	−0.46	−0.74
Norabuena *et al.* (1998)	Central Andes	43	1	S. America	62.1	−90.8	0.60	−0.004 ± 0.012	−0.283 ± 0.026	0.535 ± 0.015	−0.64	−0.47	0.57
Paul *et al.* (2001)	India	24	1	India	64.6	−37.5	1.10	0.374 ± 0.009	−0.287 ± 0.031	0.993 ± 0.013	0.64	0.48	0.77
Pérez *et al.* (2001)	Venezuela	18	1	Local	58.7	−89.0	0.64	0.006 ± 0.050	−0.330 ± 0.108	0.543 ± 0.022	−0.98	0.89	−0.91
Puntodewo *et al.* (1994)	Irian Jaya	6	1	Australia	70.8	18.1	1.00	0.311 ± 1.333	0.102 ± 1.118	0.941 ± 0.230	−1.00	0.92	−0.92
Sagiya *et al.* (2000)	Japan	918	1	Local	49.1	−71.6	0.83	0.171 ± 0.043	−0.516 ± 0.038	0.628 ± 0.042	−0.97	−0.98	0.97
Sauber *et al.* (1997)	Alaska	9	1	Local	51.2	−79.2	0.85	0.100 ± 0.076	−0.522 ± 0.052	0.661 ± 0.184	0.98	−0.99	−0.99
SCEC v.2.0[e]	S. California	318	1	N. America	48.2	−86.7	0.92	0.035 ± 0.023	−0.613 ± 0.043	0.687 ± 0.033	0.99	−0.98	−0.99
Shen *et al.* (2000)	N.E. China	71	2	NNR	65.5	−70.6	0.67	0.093 ± 0.008	−0.264 ± 0.013	0.614 ± 0.013	−0.49	−0.55	0.78
Shen *et al.* (2001)	N.W. China	42	1	ITRF97	64.2	−75.3	0.68	0.075 ± 0.005	−0.284 ± 0.004	0.608 ± 0.006	0.41	0.20	0.03
Stevens *et al.* (1999)	Sulawesi	6	1	ITRF94?	65.0	−75.4	0.71	0.076 ± 0.505	−0.292 ± 1.065	0.646 ± 0.649	−1.00	1.00	−1.00
Taylor *et al.* (1995)	New Hebrides	9	1	Australia	54.0	−5.2	1.18	0.689 ± 0.583	−0.063 ± 0.140	0.952 ± 0.243	−0.99	1.00	−0.99
Tregoning *et al.* (1998a)	E. New Guinea	15	1	ITRF94	58.2	−174.7	0.65	−0.343 ± 0.120	−0.032 ± 0.068	0.554 ± 0.025	−0.99	0.70	−0.70
Tregoning *et al.* (1998b)	Solomon Isl.	3	1	ITRF94	22.4	−24.7	2.93	2.461 ± 23.455	−1.132 ± 8.630	1.119 ± 4.993	−1.00	1.00	−1.00
Tregoning *et al.* (1999)	E. New Guinea	4	1	ITRF97	70.7	−150.8	0.59	−0.170 ± 0.274	−0.095 ± 0.167	0.557 ± 0.044	−0.99	0.73	−0.742
Trenkamp *et al.* (2002)	Northern Andes	35	1	ITRF96	62.0	−74.9	0.70	0.085 ± 0.015	−0.315 ± 0.096	0.615 ± 0.017	−0.63	0.20	−0.18

Table 1. (*Continued.*)

Source	Region	Sites[a]	σ^b	Frame[c]	Lat. (°N)	Long. (°E)	$\dot{\omega}$ (°Myr^{-1})	ω_x	ω_y	ω_z	$\rho\,(x, y)$	$\rho\,(x, z)$	$\rho\,(y, z)$
USGS[f]	Western USA	277	1	ITRF97	50.5	−74.8	0.73	0.121 ± 0.008	−0.446 ± 0.012	0.560 ± 0.011	0.92	−0.88	−0.92
Walpersdorf *et al.* (1999)	Afar Rift	2	1	ITRF91	46.2	16.3	1.34	0.893 ± 1.331	0.246 ± 1.081	0.896 ± 0.317	1.00	0.95	0.94
Wang *et al.* (2001)[g]	Central Tibet[g]	11	1	Local	66.9	−64.1	1.13	0.194 ± 0.008	−0.399 ± 0.069	1.039 ± 0.042	−0.39	−0.41	0.98
Weber *et al.* (2001)	Caribbean	10	1	ITRF97	63.5	−74.9	0.68	0.078 ± 0.010	−0.290 ± 0.013	0.604 ± 0.008	−0.61	0.13	−0.25
Yu *et al.* (1999)	Luzon–Taiwan	34	1	Eurasia	68.9	−88.0	0.89	0.011 ± 0.048	−0.321 ± 0.082	0.832 ± 0.039	−0.98	−0.95	0.96

These rotations allow the minimum least-squares fit between the model strain rate field and inferred geological strain rates and between the model velocity field and the geodetic vectors within the model Pacific frame of reference. ω_x, ω_y and ω_z are the Cartesian components of the rotation vector (deg Myr^{-1}), where x is the vector direction of 0°N, 0°E, y is the vector direction of 0°N, 90°E, and z is the vector direction of the geographic north pole; $\rho\,(x, y)$ is the correlation coefficient between x and y directions; $\rho\,(x, z)$ is the correlation coefficient between x and z directions, and $\rho\,(y, z)$ is the correlation coefficient between y and z directions.

[a]Number of geodetic sites for each study listed.

[b]Number of times the original standard errors of each listed study are multiplied.

[c]Original reference frame used by study.

[d]New standard errors are defined as $\sqrt{\sigma^2 + C^2/\Delta t^2}$, where σ is the original standard error, C is 5.5 mm yr^{-1}, and Δt is time period of each station in years.

[e]http://www.scecdc.scec.org/group_e/release.v2/.

[f]http://quake.usgs.gov/research/deformation/gps/auto/CL.html.

[g]We only used the N–S transect through central Tibet.

some sources are only available on-line (United States Geological Survey (USGS); http://quake.wr.usgs.gov/QUAKES/geodetic/gps, and the Southern California Earthquake Center (SCEC); http://www.scecdc.scec.org/group_e/release.v2). Large geodetic data sets in Asia and for the entire globe have been published very recently by Wang *et al.* (2001) and Sella *et al.* (2002), respectively, but these studies have not (yet) been included in the results presented here (with the exception of a N–S transect in Tibet that is part of the Wang *et al.* (2001) data set and that was given to us by J. Freymueller before publication of that paper).

Formal errors in geodetic velocities often underestimate the 'true' uncertainty (Johnson & Agnew 1995). This underestimation is generally owing to the fact that only 'white noise' is considered in the data analysis while effects of time-correlated noise are often not included (Mao *et al.* 1999). To acknowledge this fact and to obtain a fairly even distribution of velocity uncertainties between the different data sets we have multiplied standard errors in velocity for some of the studies by a factor of 2 or 3 (see Table 1). Alternatively, following Argus & Gordon (1996) a time-dependent velocity variance σ_{new} is defined, where $\sigma_{\text{new}} = \sqrt{\sigma^2 + C^2/\Delta t^2}$ and Δt is in years, such that for sites on the same plate the requirement of plate rigidity is met. We apply this approach to the VLBI velocities (Ma & Ryan 1998) for which we had a good knowledge of the length of the time-series for each site. We use a value of $C = 5.5$ mm yr^{-1} as suggested and used by Argus & Gordon (1996) and Larson *et al.* (1997).

To date the only Quaternary fault slip rate data used in the global model are from central Asia (England & Molnar 1997; Holt *et al.* 2000a and references therein). Although an extensive set of Quaternary fault slip rate data is available for the western United States (e.g. Peterson & Wesnousky 1994; Peterson *et al.* 1996; Shen-Tu *et al.* 1999) these data are not used in this model because of the large amount of available geodetic velocities in this region. That is, in the western United States the geodetic data alone will suffice to accurately describe ongoing present-day deformation at a scale of resolution we are seeking within a global framework.

Owing to the absence of a global data set of slip rate estimates, it is currently not possible to obtain a global strain rate field that reflects the long-term deformation pattern in diffuse plate boundary zones. On the other hand, for some plate boundary zones (e.g. western United States and the eastern Mediterranean) there are sufficient geodetic velocity measurements to constrain the strain rate field associated with ongoing motions reasonably accurately. In most cases, however, strain rate estimates from geodetic velocities will be more laterally distributed than long-term geological strain rates (e.g. Shen-Tu *et al.* 1999), due to effects of elastic loading of the lithosphere. Nevertheless, over sufficient length-scales, of the order of the width of plate boundary zones, geodetic velocities are often indistinguishable from relative plate velocities (e.g. Stein 1993; Shen-Tu *et al.* 1998; Kreemer *et al.* 2000b). We perform a smoothing of the geological strain rates over an appropriate length-scale ∼50–100 km) such that geodetic and geological strain rates compliment each other in reflecting the ongoing horizontal deformation in areas where the lateral dimension is several times larger than the elastic thickness. Geological strain rates add especially useful kinematic constraints in areas where geodetic data are limited or absent. However, as a consequence of combining these different data sets, the resolution for the global strain rate model has a lower limit of ∼50–100 km. Moreover, we do not attempt to solve for slip on individual faults. To avoid modelling of temporal changes in strain rate due to co-seismic and post-seismic relaxation of the crust, we

have not included any geodetic velocity that reflects a significant component of co- and post-seismic deformation.

4 GLOBAL STRAIN RATE MODEL

In determining a global strain rate model we seek a best fit between model velocities and 3000 observed velocities (the reduced chi-squared is 1.06) and model and geological strain rates inferred from Quaternary fault slip rates. Table 1 lists for each study the obtained angular velocity with which the original velocity vectors are rotated into the model reference frame (Pacific).

In Fig. 2 we present the second invariant of the global model strain rate field, where the second invariant is defined as $\sqrt{\dot{\varepsilon}_{\phi\phi}^2 + \dot{\varepsilon}_{\theta\theta}^2 + 2\dot{\varepsilon}_{\phi\theta}^2}$, where $\dot{\varepsilon}_{\phi\phi}$, $\dot{\varepsilon}_{\theta\theta}$ and $\dot{\varepsilon}_{\phi\theta}$ are the horizontal components of the strain rate tensor. Fig. 2 also indicates the assigned geometries of the plate boundary zones. It is evident that the highest strain rates reflect spreading along mid-oceanic ridges. Other high strain rate areas are the subduction zones along the Pacific Rim. Significantly high strain rates are apparent in diffuse boundary zones, such as central Asia and the western United States, and deformation in these zones is often heterogeneously distributed. We discuss the strain rate fields in the broad plate boundary zones of central Asia, Indian Ocean and the Aegean in more detail in the sections below describing the appropriate relative plate motions.

5 PLATE MOTIONS AND PLATE BOUNDARY DEFORMATION

The motions of most major plates are well constrained by a model velocity field obtained in a least-squares fit to the observed geodetic velocities for those plates. Fig. 3 shows the locations of the sites used in this study that are assumed to be located on a stable plate/block. Table 2 shows the reduced chi-squared for each plate for which the motion has been measured at a minimum of two positions. The plates that are defined in the model, but for which motions are not directly measured using geodetic velocities, are the Caroline, Capricorn, Cocos, Juan de Fuca, Rivera and Scotia plates. Consequently, plate motion results for these plates are currently uncertain and not presented. Table 3 displays the angular velocities of all (constrained) plates with respect to the Pacific Plate, whereas angular velocity vectors describing relative motion between selected plate pairs are shown in Table 4. For comparison, Table 4 also contains relative rotation vectors from the NUVEL-1A plate motion model (DeMets *et al.* 1994a) and from Sella *et al.* (2002) who have presented the most extensive set of geodetically derived plate motions to date.

5.1 Pacific–North America

The motion between the Pacific (PA) and North American (NA) plates has been widely studied (e.g. DeMets *et al.* 1987; Argus & Gordon 1990; Ward 1990; Antonelis *et al.* 1999; DeMets & Dixon 1999), because of the implications of this motion for plate boundary deformation and seismic hazard mitigation in California and Alaska (e.g. Minster & Jordan 1987; Humphreys & Weldon 1994; Shen-Tu *et al.* 1998). The angular velocity found here describing PA–NA motion (50.8°S, 102.2°E, 0.77°Myr^{-1}) is close to, although slightly faster than, the NUVEL-1A result. However, our Euler vector is significantly more western and at a lower rate than the geodetic estimates obtained by Larson *et al.* (1997) and Crétaux *et al.* (1998). Kreemer *et al.* (2000a) speculated that the different pole location found by others could be (partly) explained by the inclusion of the velocity at Fairbanks, Alaska, in the estimation of North America motion, which results in a PA–NA Euler pole more easterly and with a higher rotation rate. Kreemer *et al.* (2000a) found that a significantly better fit to observed North American velocities is obtained when Fairbanks is considered to lie within the PA–NA plate boundary zone, which is what we have assumed here. Nome in western Alaska (Ma & Ryan 1998) does not appear to be part of the North American Plate either. A similar conclusion was found by Argus & Gordon (1996). The residual velocity vector we find at Nome with respect to North America is 4.4 mm yr^{-1} towards S43°E. This difference is significant at the 95 per cent confidence level. When the observed velocity at Nome is taken out of the model, a better fit to the observed velocities in the eastern part of the North American Plate is obtained, but the PA–NA rotation vector remains unaffected. (In fact, the PA–NA angular velocity changes insignificantly when all North American stations west of 104°W are excluded.) Nome is located near the Bering Strait where seismicity levels are relatively high (e.g. Biswas *et al.* 1986). Seismicity here possibly delineates the northeastern boundary of the proposed independent 'Bering block' (Mackey *et al.* 1997). Initial results using the velocity obtained by Kogan *et al.* (2000) at Bilibino in eastern Siberia (750–1000 km east of the (diffuse) NA–Eurasia (EU) plate boundary zone Chapman & Solomon 1976) led to a significant residual velocity for this site as well. However, given a new revised 5 yr velocity estimate at Bilibino (M. Kogan, pers. comm. 2002), this station now appears to be part of rigid NA.

PA–NA motion within our model velocity field (Fig. 4) has a magnitude of 53.3 ± 1.0 mm yr^{-1} towards N56°W ±1° at a point on the Pacific Plate just off-shore of Cabo San Lucas at the southern tip of Baja California (22°N, 111°W) (Baja California itself is assumed to be part of the PA–NA plate boundary), 48.8 ± 1.0 mm yr^{-1} in a direction of N44°W ± 1° off-shore of southern California (32°N, 118°W), 48.2 ± 1.0 mm yr^{-1} towards N37°W ±1° near San Francisco (37.5°N, 123°W) and 59.0 ± 1.0 mm yr^{-1} towards N28°W ± 1° south of Kodiak Island (54°N, 153°W) (here and hereafter, uncertainties represent 95 per cent confidence limits). Our results predict a PA–NA motion along southern California and Baja California that is about 2–3 mm yr^{-1} faster than NUVEL-1A. This result is consistent with the GPS results found by others (DeMets & Dixon 1999; Beavan *et al.* 2002; Sella *et al.* 2002).

Along the PA–NA plate boundary we find that model velocities are directed anticlockwise from the NUVEL-1A PA–NA motion direction, with a maximum discrepancy of almost 3° in central and southern California (Fig. 4). This result is consistent with the 2°–3° anticlockwise discrepancy in direction found by Shen-Tu *et al.* (1999) and Larson *et al.* (1997) based on GPS measurements. Based on the summation of Quaternary fault slip rates over the entire PA–NA plate boundary zone Humphreys & Weldon (1994) and Shen-Tu *et al.* (1999) found that the Pacific Plate moves up to 6° anticlockwise from the NUVEL-1A estimate.

5.2 Caribbean–North America and Caribbean–South America

We have assumed that San Andres Island, Aves Island and St Croix (US Virgin Islands) are located on the stable Caribbean (CA) Plate (Fig. 5). Site velocities at all three locations are taken from Weber *et al.* (2001). The site at St Croix is also measured as part of the VLBI global network (Ma & Ryan 1998), as part of the GPSVEL solution, and as part of a regional GPS network in Puerto Rico (Jansma *et al.* 2000). There is an additional measured velocity at Aves Island by Pérez *et al.* (2001). Using the least-squares fitting procedure we

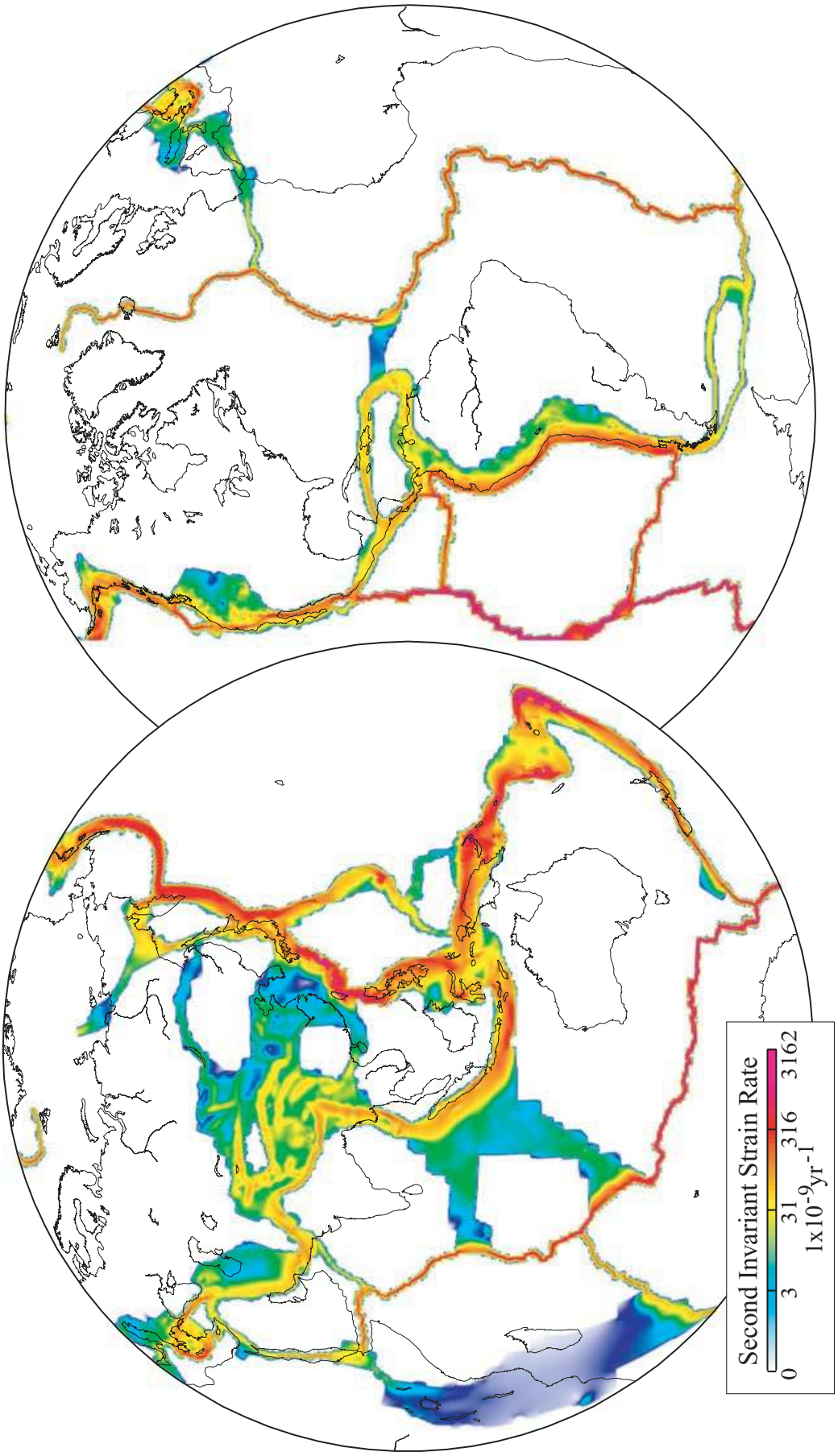

Figure 2. Contours of the second invariant of the model strain rate field determined using 3000 geodetic velocities world-wide, and Quarternary slip rates in Asia. All areas in white are assumed to behave rigidly. The contour scale is quasi-exponential.

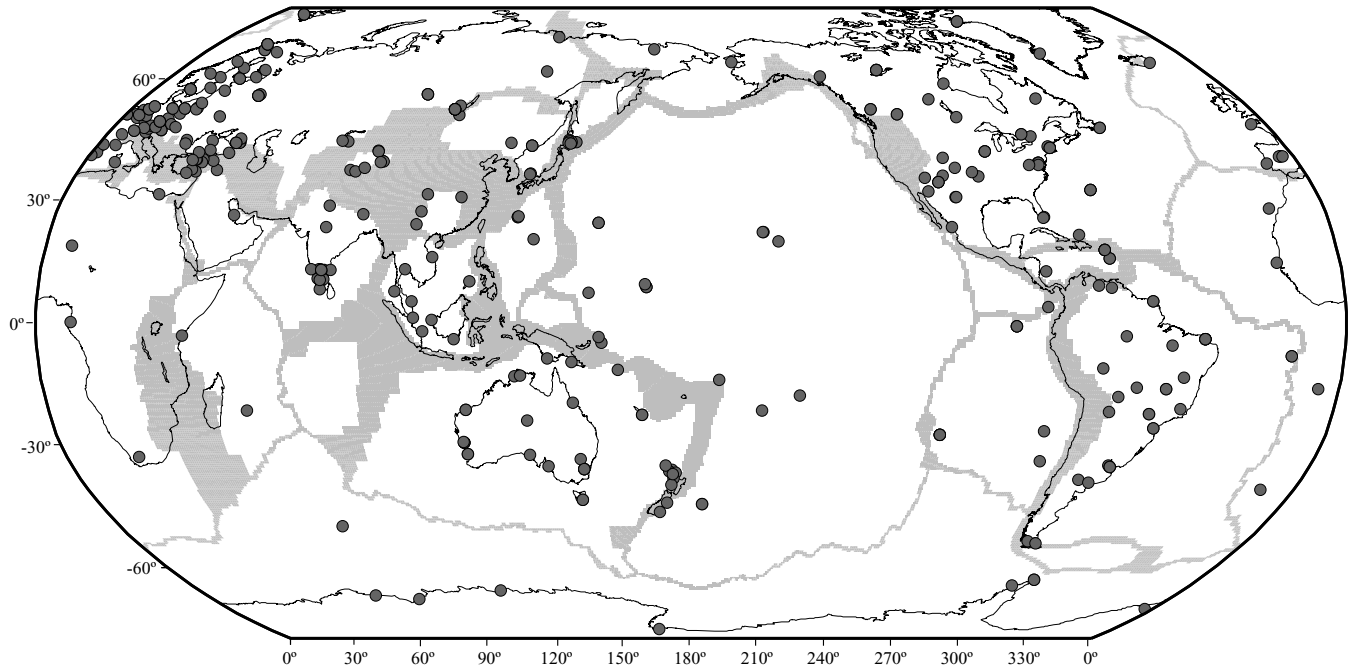

Figure 3. Locations of sites that are assumed to be located within stable plate interiors. Velocities at these sites are used to infer relative angular velocities of the respective plates. Outlined in grey are all plate boundary zones incorporated in the model.

find a reduced chi-squared of 0.50 (Table 2) for the fit between the seven geodetic velocities and the predicted model velocities (Fig. 5). No apparent evidence is found for possible intraplate deformation as was inferred by Leroy & Mauffret (1996). From our inversion we find that CA–NA motion is best described by an Euler pole at 75.3°N, 136.5°W at a rate of 0.18°Myr^{-1}, close to the result found by DeMets *et al.* (2000). With respect to the South-American (SA) Plate the Caribbean Plate moves about a pole at 53.8°N, 71.0°W at a rate of 0.26°Myr^{-1}, consistent with the result by Weber *et al.* (2001). The relatively high inferred velocity of the Caribbean Plate compared with the NUVEL-1A estimate (Fig. 5) is consistent with earlier geodetic studies (Dixon *et al.* 1998; MacMillan & Ma 1999; DeMets *et al.* 2000; Weber *et al.* 2001; Sella *et al.* 2002). Following Dixon *et al.* (1998) we believe that the discrepancy in rate can be explained by a systematic error in the NUVEL-1A estimate of Caribbean Plate motion. The cause of the error is probably the inclusion of some earthquake slip-vectors (especially along the Middle America trench) that may not reflect actual relative plate motion direction (Deng & Sykes 1995). This idea is supported in a study by DeMets (1993) in which he found a significant increase in the rate of CA–NA motion when earthquake data are omitted from the NUVEL-1 model (DeMets *et al.* 1990).

Table 2. Goodness of fit of model velocities to geodetic velocities.

Plate	N^{vel}	N^{sites}	N^{study}	χ^2
Amurian	7	6	6	1.31
Anatolia	10	9	2	1.02
Antarctica	9	8	2	0.77
Arabia	2	2	2	0.36
Australia	34	26	10	0.90
Caribbean	7	3	5	0.50
Eurasia	122	78	13	1.05
India	19	14	6	1.66
Nazca	10	5	5	1.48
North America	57	39	7	1.03
Nubia	8	8	3	0.54
Okhotsk	10	10	1	0.97
Pacific	18	15	6	1.26
Philippine Sea	4	3	3	3.37
Somalia	2	2	2	0.86
South America	33	22	7	0.73
South China	4	4	2	2.16
Sunda	9	9	2	3.11
Tarim	8	8	2	1.13
Global Total	3000	2749	50	1.06

χ^2 is the reduced chi-squared, calculated by dividing the weighted squared misfit by the number of degrees of freedom (which equals the number of observed velocity components at each plate minus 3). N^{vel}, number of included observed velocity vectors for respective plate; N^{sites}, number of locations on respective plate for which observed velocity vectors are included; N^{study}, number of studies from which velocity vector estimates are used for the respective plate.

5.3 South America–North America

Although the separateness of the North and South American plates has been recognized for a long time (e.g. Ball & Harrison 1970), estimates for the relative motion of this plate pair were for a long time solely based on plate circuit closures (e.g. Minster & Jordan 1978; DeMets *et al.* 1990). Direct observations using GPS have confirmed that North and South America are distinct plates (Argus & Heflin 1995; Larson *et al.* 1997; Dixon & Mao 1997; Crétaux *et al.* 1998; Sella *et al.* 2002). Geodetic velocities in our model are fitted well on both the North and South American plates (reduced chi-squared is 1.03 and 0.73, respectively, Table 2), including at stations on the South American Plate as far east as Ascension Island (GPSVEL) and as far south as Punta Arenas (Bevis *et al.* 1999) and Rio Grande, Argentina (GPSVEL). We obtain an SA–NA angular velocity vector (13.9°S, 126.2°E, 0.15°Myr^{-1}) close to the estimate by Dixon & Mao (1997) and Sella *et al.* (2002), which are the only two studies that include a fair number of stations on both plates.

Table 3. Angular velocities of most plates with respect to the Pacific Plate.

Plate	Lat. (°N)	Long. (°E)	$\dot{\omega}$ (°Myr^{-1})	ω_x	ω_y	ω_z	$\rho\,(x, y)$	$\rho\,(x, z)$	$\rho\,(y, z)$
Amurian	64.1	−84.8	0.945	0.038 ± 0.008	−0.411 ± 0.011	0.850 ± 0.015	−0.60	−0.67	0.85
Anatolia	56.1	11.8	1.847	1.007 ± 0.069	0.211 ± 0.045	1.534 ± 0.067	0.99	0.99	0.99
Antarctica	65.8	−87.3	0.881	0.017 ± 0.005	−0.360 ± 0.005	0.803 ± 0.009	0.27	−0.18	−0.35
Arabia	63.4	−33.7	1.134	0.422 ± 0.037	−0.281 ± 0.040	1.014 ± 0.032	0.96	0.94	0.94
Australia	62.2	4.4	1.063	0.494 ± 0.006	0.038 ± 0.005	0.940 ± 0.005	−0.22	0.30	−0.52
Caribbean	56.4	−82.2	0.924	0.069 ± 0.015	−0.506 ± 0.029	0.770 ± 0.011	−0.87	0.71	−0.82
Eurasia	62.8	−82.7	0.923	0.054 ± 0.005	−0.418 ± 0.003	0.821 ± 0.005	0.44	0.08	−0.11
India	63.2	−42.8	1.094	0.362 ± 0.007	−0.336 ± 0.022	0.977 ± 0.010	0.60	0.44	0.78
Nazca	55.2	−89.6	1.271	0.006 ± 0.008	−0.725 ± 0.017	1.044 ± 0.009	0.37	0.19	0.60
N. America	50.8	−77.9	0.768	0.102 ± 0.004	−0.474 ± 0.004	0.595 ± 0.004	0.34	−0.22	−0.49
Nubia	61.1	−76.0	0.939	0.110 ± 0.011	−0.440 ± 0.006	0.822 ± 0.008	0.03	0.27	−0.12
Okhotsk	−3.2	−51.6	1.058	0.657 ± 0.130	−0.827 ± 0.094	−0.060 ± 0.164	−0.99	−0.99	0.99
Philippine Sea	−2.1	−42.5	0.833	0.614 ± 0.186	−0.563 ± 0.206	−0.031 ± 0.132	−0.99	−0.98	0.98
Somalia	61.2	−79.2	0.951	0.085 ± 0.008	−0.430 ± 0.007	0.833 ± 0.004	0.78	−0.50	−0.52
S. America	57.2	−86.9	0.667	0.019 ± 0.006	−0.361 ± 0.006	0.560 ± 0.005	−0.38	−0.39	0.20
S. China	73.0	−96.9	1.028	−0.036 ± 0.010	−0.298 ± 0.028	0.983 ± 0.016	−0.81	−0.80	0.92
Sunda	58.6	−82.2	1.028	0.073 ± 0.007	−0.531 ± 0.014	0.877 ± 0.007	−0.47	−0.24	0.34
Tarim	26.6	−83.1	1.002	0.108 ± 0.007	−0.890 ± 0.036	0.449 ± 0.030	0.55	0.53	0.97

Angular velocities are only shown for plates for which the motions are constrained directly by at least one geodetic velocity. Consequently, no angular velocities are given for the Scotia, Rivera, Capricorn, Caroline, Cocos and Juan de Fuca plates. Angular velocities are presented in °Myr^{-1}; ω_x, ω_y, and ω_z are the Cartesian components of the rotation vector (°Myr^{-1}), where x is the vector direction of 0°N, 0°E, y is the vector direction of 0°N, 90°E, and z is the vector direction of the geographic north pole; $\rho\,(x, y)$ is the correlation coefficient between x and y directions; $\rho\,(x, z)$ is the correlation coefficient between x and z directions, and $\rho\,(y, z)$is the correlation coefficient between y and z directions.

In our model we assume the diffuse SA–NA plate boundary zone between the Lesser Antilles and the Mid-Atlantic Ridge to be ∼325–500 km wide and to include a zone of anomalous ridge and trough features that may be related to SA–NA boundary deformation (Müller & Smith 1993). The boundary zone also includes the 50–20 fracture zone, which has been suggested to be the SA–NA plate boundary (Roest & Collette 1986). The observed seismicity in the boundary zone is low, but significantly higher in comparison with other areas in the Atlantic Ocean (e.g. Bergman & Solomon 1980; Bergman 1986; Wysession *et al.* 1995), and for three events a moment tensor solution is available (e.g. Stein *et al.* 1982). These three events are located in the western part of the boundary zone and the moment tensors are consistent in style; all three events show roughly N–S-trending *P* axes, and events are characterized by a combination of thrusting and right-lateral strike-slip faulting along WNW-trending fault planes, subparallel to regional fracture zones (Stein *et al.* 1982; Bergman 1986). Our model results places the NA–SA rotation pole within the assumed NA–SA plate boundary zone. Although predicted relative motions in the plate boundary zone have a relatively high uncertainty due to the proximity of the rotation pole, predicted NA–SA relative motions are consistent in direction with the moment tensor solutions, albeit the total relative motion does not exceed 2 mm yr^{-1}. However, due to the lack of additional moment tensor solutions for the (very few) events in the boundary zone and, again, because the Euler pole is very close to the boundary zone, the exact nature of the seismotectonics in this area remains uncertain.

5.4 Nazca–South America and Nazca–Pacific

From plate reconstructions (Pardo-Casas & Molnar 1987) and new seafloor data (Somoza 1998), it has been suggested that Nazca (NZ) Plate motion has slowed down gradually since 20–25 Ma. Recently, the decelerating of the Nazca Plate has been confirmed by geodetic measurements (Larson *et al.* 1997; Angermann *et al.* 1999; Norabuena *et al.* 1999). Our angular velocity vectors describing NZ–SA (53.1°N, 92.1°W, 0.61°Myr^{-1}) and NZ–PA (55.2°N, 89.6°W, 1.27°Myr^{-1}) relative motion (Table 4), confirm slower relative motions compared with the NUVEL-1A model as was noted before by others (Angermann *et al.* 1999; Norabuena *et al.* 1999; Kreemer *et al.* 2000; Sella *et al.* 2002). The NZ–SA Euler pole yields convergence directions along the South American margin that are remarkably indistinguishable from the predicted NUVEL-1A motion directions. Convergence rates, on the other hand, range from 58 ± 2 mm yr^{-1} in Ecuador to 67 ± 2 mm yr^{-1} in Central Chile, which is, respectively, 18 and 16 per cent slower than the NUVEL-1A predicted convergence rates. Similarly, we find that predicted spreading rates along the East Pacific Rise between the Nazca and Pacific plates are indistinguishable in direction from the NUVEL-1A model, but ∼9 mm yr^{-1}, or ∼7 per cent, slower.

Because the NZ–PA relative motion is very well constrained in the NUVEL-1A model, it is unlikely that the discrepancy between the geological and geodetic speed of the Nazca Plate is the result of a systematic error in the NUVEL-1A model. Instead, the relatively low present-day speed of the Nazca Plate compared with its speed over the last 3 Myr hints at a true deceleration of the plate (Norabuena *et al.* 1999). Norabuena *et al.* (1999) suggested that slowing down of the Nazca Plate may be the result of increased drag between the subducting Nazca and overriding South American Plate caused by thickening of South America's leading edge owing to growth of the Andes, resulting in 'flat-slab' subduction. Because 'flat-slab' subduction is not observed uniformly along the NZ–SA boundary (e.g. Stauder 1975; Barazangi & Isacks 1976) a more likely mechanism for 'flat-slab' subduction is the subduction of buoyant 'aseismic' ridges (Vogt 1973; Vogt *et al.* 1976; Kelleher & McCann 1976). The Nazca Plate seems somewhat outstanding in this respect since it is floored by several 'aseismic' ridges that are all being subducted beneath South America. Pilger (1981) pointed out the correlation between zones of low-angle subduction and places where the Nazca and Juan Fernández ridges subduct underneath

Table 4. Relative angular velocities for selected plate pairs.

Plate pair	Model	Lat. (°N)	Long. (°E)	$\dot{\omega}$ (°Myr^{-1})	σ_{max} (deg)	σ_{min} (deg)	ψ	σ_{ω} (°Myr^{-1})
EU–NA	A	71.8	130.6	0.238	0.8	0.6	9	0.003
	B	62.4	135.8	0.21	4.1	1.3	−11	0.01
	C	68.1	136.4	0.245	1.5	0.8	−38	0.004
PA–NA	A	−50.8	102.2	0.768	0.3	0.2	−87	0.005
	B	−48.7	101.8	0.75	1.3	1.2	61	0.01
	C	−50.4	107.9	0.755	0.6	0.4	79	0.004
SA–NA	A	−13.9	126.2	0.145	2.0	1.1	17	0.007
	B	−16.3	121.9	0.15	5.9	3.7	9	0.01
	C	−12.9	129.6	0.171	2.7	1.3	10	0.009
NU-NA	A	81.1	77.6	0.230	2.6	1.5	87	0.008
	B	78.8	38.3	0.24	3.7	1.0	77	0.01
	C	77.9	104.8	0.213	2.0	1.2	−64	0.004
OK–NA	A	−44.9	−32.4	0.928	1.1	0.9	41	0.224
	C	−56.7	−33.0	0.305	11.8	1.7	−18	0.121
CA–NA	A	75.3	−136.5	0.181	10.5	1.6	−77	0.013
	B	74.3	153.9	0.10	24.7	2.6	52	0.03
	C	75.5	−154.6	0.180	10.9	1.3	88	0.008
CA–SA	A	53.8	−71.0	0.260	4.2	1.2	−11	0.026
	B	50.0	−65.3	0.18	14.9	4.3	−2	0.03
	C	52.8	−66.3	0.267	5.4	1.4	−5	0.021
NZ–SA	A	53.1	−92.1	0.605	1.7	0.7	5	0.008
	B	56.0	−94.0	0.72	3.6	1.5	−10	0.02
	C	52.1	−91.2	0.633	3.1	1.2	8	0.009
AN–SA	A	89.5	159.4	0.243	1.8	1.1	37	0.009
	B	86.4	−40.7	0.26	3.0	1.2	−24	0.01
	C	84.6	−128.1	0.240	3.5	1.4	−80	0.011
NU–SA	A	65.4	−41.0	0.288	2.1	1.5	−29	0.009
	B	62.5	−39.4	0.31	2.6	0.8	−11	0.01
	C	62.7	−42.0	0.277	3.1	1.3	−2	0.006
AN–PA	A	65.8	−87.3	0.881	0.4	0.3	73	0.009
	B	64.3	−84.0	0.87	1.2	1.0	81	0.01
	C	66.0	−85.4	0.857	0.6	0.4	88	0.011
AU–PA	A	62.2	4.4	1.063	0.3	0.3	13	0.006
	B	60.1	1.7	1.07	1.0	0.9	58	0.01
	C	61.4	6.2	1.080	0.6	0.4	62	0.008
NZ–PA	A	55.2	−89.6	1.271	0.8	0.3	9	0.008
	B	55.6	−90.1	1.36	1.9	0.9	−1	0.02
	C	55.4	−87.3	1.267	1.6	0.5	17	0.008
PH–PA	A	−2.1	−42.5	0.833	6.3	1.5	13	0.268
	B	−1.2	−45.8	0.96	–	–	–	–
	C	−4.6	−41.7	0.874	1.7	0.6	15	0.049
NZ–AN	A	33.4	−91.8	0.437	2.1	0.9	7	0.013
	B	40.5	−95.9	0.52	4.5	1.9	−9	0.02
	C	35.1	−89.1	0.453	4.0	1.0	15	0.015
AN–AU	A	−12.4	−140.1	0.636	0.9	0.5	25	0.004
	B	−13.2	−141.8	0.65	1.3	1.0	63	0.01
	C	−14.7	−140.3	0.653	1.6	0.8	33	0.004
IN–AU	A	5.2	−109.5	0.398	0.8	0.8	−25	0.019
	B	5.6	−102.9	0.30	7.4	3.1	43	0.07
	C	4.4	−108.0	0.409	4.7	1.7	−15	0.066
NU–SO	A	−23.3	21.9	0.028	13.6	10.9	−63	0.044
	C	−35.5	24.0	0.085	4.9	3.1	−19	0.005
NU–EU	A	1.1	−21.3	0.060	6.9	5.8	21	0.010
	B	21.0	−20.6	0.12	6.0	0.7	−4	0.02
	C	−18.2	−20.0	0.062	9.5	3.7	17	0.005
AU–EU	A	10.7	46.0	0.645	0.5	0.2	−53	0.003
	B	15.1	40.5	0.69	2.1	1.1	−45	0.01
	C	12.6	46.2	0.640	1.3	0.5	−52	0.005
IN–EU	A	25.9	15.0	0.355	3.7	0.9	75	0.006
	B	24.4	17.7	0.51	8.8	1.8	−79	0.05
	C	28.6	11.6	0.357	14.4	1.1	89	0.033
AR–EU	A	26.2	20.4	0.437	3.7	0.9	77	0.023
	B	24.6	13.7	0.50	5.2	1.7	−72	0.05
	C	26.2	22.9	0.427	2.1	1.1	76	0.029

Table 4. (*Continued*.)

Plate pair	Model	Lat. (°N)	Long. (°E)	$\dot{\omega}$ (°Myr^{-1})	σ_{max} (deg)	σ_{min} (deg)	ψ	σ_{ω} (°Myr^{-1})
AT–EU	A	32.0	33.4	1.346	0.7	0.2	1	0.105
	C	26.6	34.4	0.833	20.0	0.7	−5	0.871
AM–EU	A	58.8	157.5	0.034	5.5	3.4	−87	0.013
	C	44.2	158.8	0.107	33.3	6.6	88	0.100
SC–EU	A	47.3	126.8	0.220	8.7	2.4	67	0.021
	C	41.9	−124.0	0.087	65.1	6.6	−50	0.006
SU–EU	A	26.0	−80.4	0.128	10.8	4.6	31	0.010
	C	8.8	−75.5	0.181	5.4	2.2	4	0.078
TA–EU	A	−38.1	−83.4	0.604	0.8	0.4	75	0.046

Angular velocities are for the first plate relative to the second. Model A is the model obtained from a least-squares fit to 3000 geodetic velocities as well as to geological strain rates inferred from Quaternary fault slip rates in central Asia. Model B is NUVEL-1A (DeMets et al. 1994a), and model C is by Sella *et al.* (2002). Plate abbreviations: EU, Eurasia; NA, North America; PA, Pacific; SA, South America; CA, Caribbean; OK, Okhotsk; PH, Philippine Sea; NZ, Nazca; AN, Antarctica; AU, Australia; IN, India; AR, Arabia; AT, Anatolia; AM, Amurian; SC; South China; SU, Sunda; TA, Tarim; NU, Nubia; SO, Somalia. For model C Africa is assumed to be the same as Nubia. σ_{max} and σ_{min} are the semi-major and semi-minor axes of the 2-D 1σ error ellipse and ψ is the azimuth of the semi-major axis. For 95 per cent confidence multiply standard errors by 2.45.

southern Peru and central Chile, respectively. Gutscher *et al.* (1999) determined a similar correlation for Ecuador where the 'aseismic' Carnegie Ridge subducts. It has been inferred that subduction of the Carnegie, Nazca and Juan Fernández ridges all initiated 8–9 Myr (Cande 1985; Von Huene *et al.* 1997; Gutscher *et al.* 1999), which correlates well with the estimated 31 mm yr^{-1} decrease in NZ–SA convergence rate between 10.8 and 4.9 Ma (Somoza 1998). Similarly, the ∼14 mm yr^{-1} decrease in convergence rate since 3 Ma, based on a comparison of the NUVEL-1A estimated rate with the GPS measurements (Norabuena *et al.* 1999; Angermann *et al.* 1999) and our result, could be a reflection of the continuation of the subduction process of these aseismic ridges. In addition, the repeated subduction of ridge crest segments of the active Chile ridge underneath southern Chile since 14 Ma (Cande & Leslie 1986; Ramos & Kay 1992) could have also contributed to the deceleration of the NZ–SA plate motion.

5.5 Australia–Pacific

In the NUVEL-1A model the Australia (AU)–PA plate pair is another example for which the relative motion is inferred indirectly through plate circuit closure due to lack of useful geological data along its boundary. A good knowledge of relative motion along the AU–PA boundary is, however, of great interest in studying some of the segments along this boundary; the Tonga–Kermadec subduction zone that is the source of the majority of (deep) global seismicity, the Alpine fault in New Zealand, and the Macquarie ridge along which one of the largest earthquakes ($M_W = 8.2$) in the last couple of decades occurred. Until recently, studies of the PA–AU relative plate motion were hindered by a limited distribution of sites on the Australian and Pacific plates (e.g. Smith *et al.* 1994; Argus & Heflin 1995; Larson *et al.* 1997; Crétaux *et al.* 1998). Fortunately, recent studies by Sella *et al.* (2002) and Beavan *et al.* (2002), as well as this study, have had access to a much wider distribution of sites on these plates (Fig. 3). Beavan *et al.* (2002) found that velocities of stations 5508 and OUSD in eastern South Island, New Zealand, do not represent Pacific motion. We find that the velocities of these two stations, that we have assumed to be located on the Pacific Plate but that we have taken from the Beavan & Haines (2001) study instead of Beavan *et al.*'s (2002) paper, are consistent with rigid plate motion. We obtain an angular velocity vector for PA–AU motion of 62.2°S, 175.6°W, 1.06°Myr^{-1} (Table 4). Our result is within the 95 per cent confidence limit of the NUVEL-1A estimate. This finding is somewhat surprising, because there have been indications that the present-day PA–AU Euler pole is located about 5° south of the NUVEL-1A pole (Larson *et al.* 1997; Crétaux *et al.* 1998), consistent with the result from plate reconstructions that the pole location has moved southward since at least 49 Ma (Molnar *et al.* 1975; Weissel *et al.* 1977; Stock & Molnar 1982; Sutherland 1995). However, uncertainties in stage poles have been large and generally overlap for different stages. Furthermore, the GPS-derived Euler pole by Larson *et al.* (1997) has been suggested to be incorrect (Beavan *et al.* 1999) based on discrepancies between predicted motions of New Zealand's South Island and locally observed GPS velocities. Our result suggests that the PA–AU angular velocity has changed insignificantly since at least 3 Ma. A similar conclusion was reached by Beavan *et al.* (2002). Nevertheless, because of the proximity of the PA–AU pole to the PA–AU plate boundary zone, very small variations in the pole location can result in significant variations in predicted velocities along the boundary; we find that our model predicts velocities from Tonga to Macquarie that are 2–5 mm yr^{-1} faster than the NUVEL-1A prediction. The azimuths of the predicted slip vectors along the PA–AU plate boundary zone are within the 95 per cent confidence level of slip-vectors predicted by the NUVEL-1A model, with the only exception being for the most southern part of the Macquarie Ridge Complex where our model predicts a PA–AU velocity of up to 9° more westward than the NUVEL-1A direction.

5.6 India–Eurasia

Estimating the present-day motion of the Indian (IN) Plate is of great importance for continental deformation studies in central and southeast Asia (e.g. England & Houseman 1986; Holt *et al.* 1995; England & Molnar 1997). Because IN–EU relative plate motion cannot be inferred directly from conventional plate motion data, space geodetic velocities are of special interest here. The southernmost part of the Indian subcontinent is particularly well covered by stations (Paul *et al.* 2001). Besides a number of velocity estimates at Bangalore from a series of studies, our model also includes

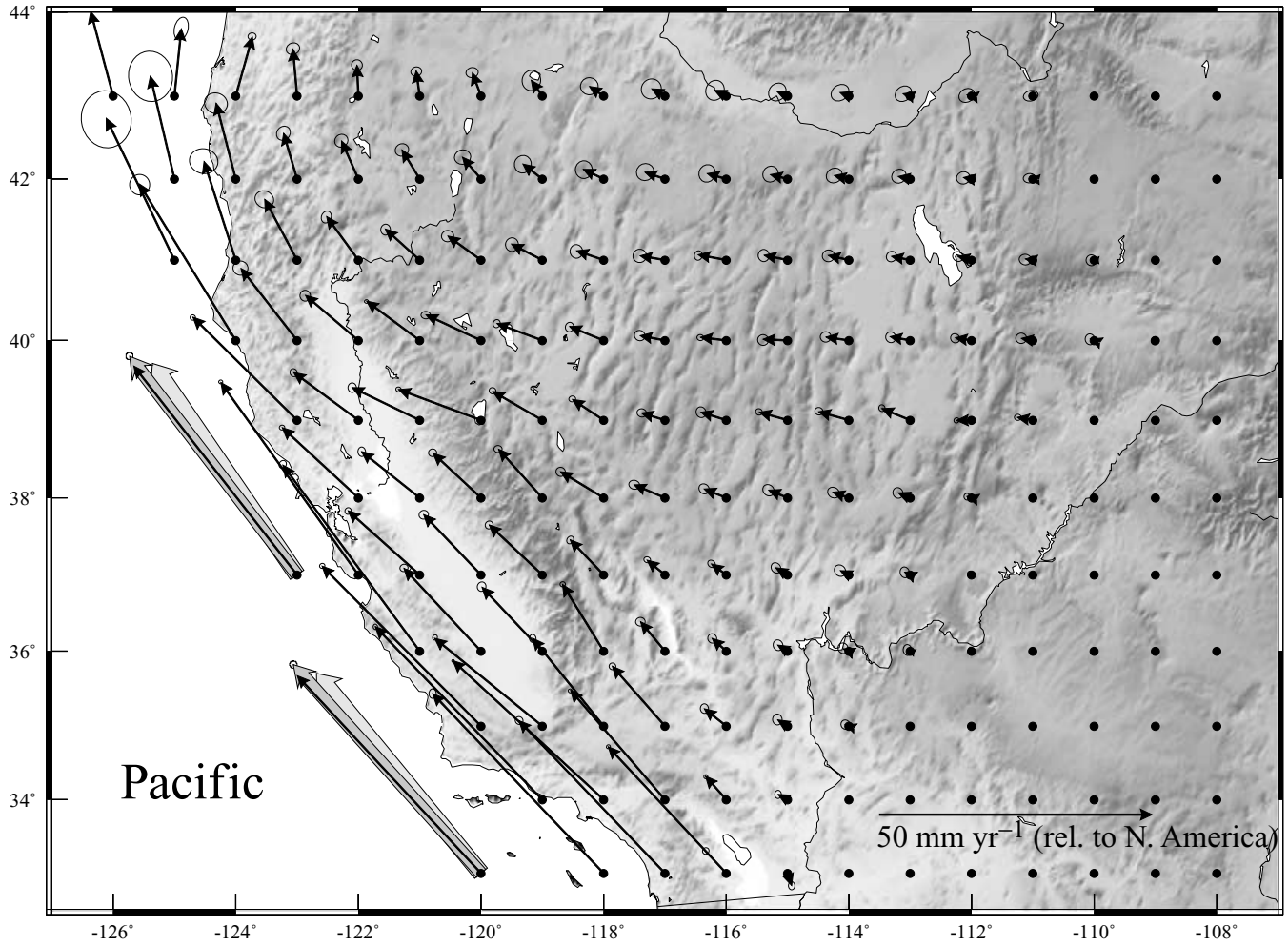

Figure 4. Black vectors are model velocities in the western United States with respect to stable North America determined at regular points. error ellipses represent 1σ uncertainty. Also shown for two locations off-shore California are the Pacific–North America velocity estimates from the NUVEL-1A model (light grey vector) and from DeMets & Dixon (1999) (dark grey vector).

velocity estimates at Bhopal and Delhi (JNUC) (Paul *et al.* 2001) and at Biratnagar (Larson *et al.* 1999) (Fig. 6a). Biratnagar is located ∼100 km south of the active Himalayan thrust belt, but we found no evidence that the velocity at this station contains any significant component of elastic deformation.

We find that IN–EU model velocity is best described by an Euler pole at 25.9°N and 15.0°E with a rotation rate of 0.36°Myr^{-1}. The pole location is within 95 per cent confidence limits of both the NUVEL-1A result (Table 4) and the pole location by Paul *et al.* (2001) (25.6°N, 11.1°E, 0.44°Myr^{-1}), but the expected rotation rate is, respectively, 0.15 and 0.08°Myr^{-1} slower. Our result is consistent with the findings of Sella *et al.* (2002) and with previous modelling results using GPS and fault slip rates in central and southeast Asia (Holt *et al.* 2000a; Holt *et al.* 2000b). Gordon *et al.* (1999) investigated a possible systematic error in NUVEL-1A India motion; they re-analysed spreading rate and transform fault data while redefining plate closure circuits and embedding a divided African Plate in their modelling. Gordon *et al.* (1999) found an angular velocity vector that yields a velocity at Bangalore with respect to Eurasia of 37 mm yr^{-1} with an azimuth of N31°E, which suggests that India's motion has not slowed down since 3 Ma, but merely that the NUVEL-1A IN–EU estimate is erroneous. Our model velocity at Bangalore with respect to Eurasia is 34.1 ± 1.2 mm yr^{-1} towards N23°E ± 2°. This model velocity is consistent with results by Holt *et al.* (2000a), Wang *et al.* (2001) and most of the six used GPS vectors at this site (with the exception of the estimate by Shen *et al.* 2000). However, in several cases the GPS velocities at Bangalore are only consistent with the model velocity after the GPS velocities have been rotated from their original Eurasian reference frame into the best-fitting model Eurasian reference frame presented here. We find that the discrepancy between our model Eurasian reference frame and the Eurasian reference frame defined by others exists mainly for studies that used the NUVEL-1A no-net-rotation (NNR) model (Argus & Gordon 1991; DeMets *et al.* 1994a) to convert from an ITRF to a tectonic reference frame. The current NNR model, however, does not adequately describe the motion of most plates in a present-day NNR reference frame (Kreemer & Holt 2001). We believe that this is also the reason why the IN–EU rotation rate estimate by Paul *et al.* (2001) is relatively high, yielding a velocity of 44 mm yr^{-1} at Bangalore. At Biratnagar, in northern India (26.48°N, 87.26°E), we infer a convergence rate of 35.5 ± 1.3 mm yr^{-1}, and a convergence direction of N17°E ± 2°. Our result implies an IN–EU convergence rate that is 14–15 mm yr^{-1} lower than predicted from the NUVEL-1A model.

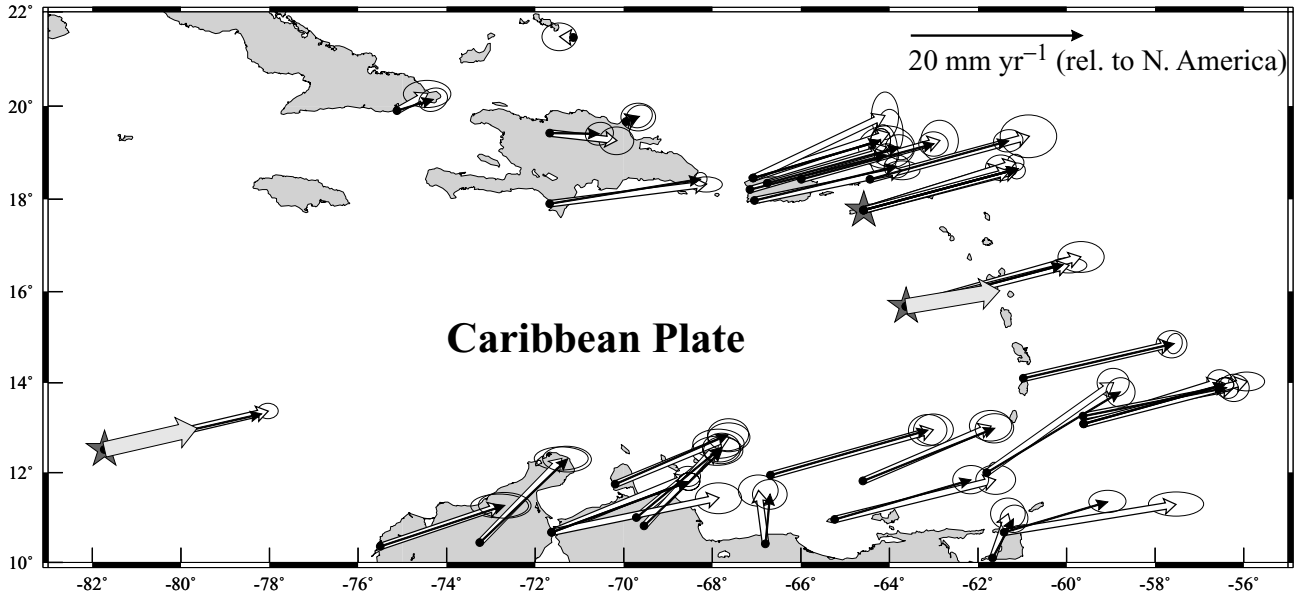

Figure 5. Model (black vectors) and geodetic velocities (white vectors) in the Caribbean. Velocities are with respect to the model North America reference frame (i.e. geodetic velocities have been rotated from their original reference frame into the NA reference frame) and error ellipses represent 1σ uncertainty. Geodetic velocities have been taken from the following studies: Ma & Ryan (1998), Dixon *et al.* (1998), Jansma *et al.* (2000), Weber *et al.* (2001), Pérez *et al.* (2001), Trenkamp *et al.* (2002), GPSVEL. Velocities at sites marked by a star were used to infer the angular velocity of the Caribbean Plate. Wide grey vectors indicate NUVEL-1A CA–NA motion (DeMets *et al.* 1994a).

5.6.1 Strain rate and velocity field in central Asia

Central Asia is the only region in the current global model in which we have attempted to not only fit geodetic velocities but also geological strain rates inferred from Quaternary fault slip rates. Fig. 6(a) shows model and observed velocities with respect to model Eurasia. Recently, Wang *et al.* (2001) combined many of the same regional studies in China that we have incorporated in this study (their study, however, combined raw data, whereas we combine velocity vectors) and their solution is very similar to the magnitude and directions of the geodetic vectors shown in Fig. 6(a). Fig. 6(b) contains the principal axes of the model strain rate field (black) and the geological strain rate field (white). Although we obtain a solution with a resolution of 0.5×0.6^2, for illustration purposes we show the strain rate field only as averages for larger grid areas (Fig. 6b). These larger grid areas are equal to the areas used by Holt *et al.* (2000a). Our strain rate tensor field within central Asia is, in general, similar to the result from the regional study by Holt *et al.* (2000a), but differs at two locations as a result of the use of new geodetic data (Chen *et al.* 2000; Shen *et al.* 2000, 2001; Bendick *et al.* 2000; Wang *et al.* 2001). Model shear rates along the Sagaing fault are higher in our result compared with that of Holt *et al.* (2000a). These high shear strain rates are a result of the SSE motion of southwestern China with respect to Siberia (Chen *et al.* 2000) (Fig. 6a). The other new result inferred from our model is the indication that a NNE-trending shear zone exists in north central Tibet (between 85°E and 90°E), subparallel to and south of the Altyn Tagh fault. Recent GPS results (Bendick *et al.* 2000; Shen *et al.* 2001) have suggested that the slip rate along the Altyn Tagh fault is roughly 9 mm yr^{-1}, significantly lower than geological estimates of 20–30 mm yr^{-1} (e.g. Peltzer *et al.* 1989). The total shear strain rates required to accommodate the 25 mm yr^{-1} of eastward motion of eastern Tibet with respect to the Tarim Basin (Fig. 6a), as indicated by GPS estimates (Heki 1996; Chen *et al.* 2000; Shen *et al.* 2000, 2001), significantly exceeds the geodetically observed slip rate, and hence shear strain rates, on the Altyn Tagh fault. The amount of additional shear strain required to accommodate the eastward motion of eastern Tibet with respect to the Tarim Basin seems to localize south of the Altyn Tagh fault on the Kun Lun fault and parallel to the westward extension of the Kun Lun fault. It is interesting to note that the epicentres of the 1997 $M_W = 7.6$ Manyi and 2001 $M_W = 7.8$ Kokoxilli earthquakes are roughly located in this zone of relatively large model shear strain rates. The moment tensor of these events are consistent with the left-lateral predicted shear strain rate direction (the Manyi event ruptured a 170 km long fault with a strike of N76°E Peltzer *et al.* 1999).

5.7 India–Australia

The separateness of the Australian and Indian plates and the diffuse nature of their mutual boundary have been established for some time (e.g. Stein & Gordon 1984; Wiens *et al.* 1985; Gordon *et al.* 1990; Royer & Chang 1991). An estimate of the relative motion between these two plates is of significant importance in studies quantifying the deformation within the Indian Ocean and understanding the relative high level of seismicity that occurs there (e.g. Gordon *et al.* 1990; Tinnon *et al.* 1995). We obtain an AU–IN Euler pole at 5.2°S and 70.5°E with a rotation rate of 0.40°Myr^{-1} (Table 4). The pole location is within 95 per cent confidence limits of the NUVEL-1A, Gordon *et al.* (1990) and DeMets *et al.* (1994b) Euler pole estimates, all of which are based on conventional plate motion data and plate circuit closure requirements. However, the rotation rate found here, as well as by Sella *et al.* (2002), is 0.09–0.11°Myr^{-1} faster than these prior estimates.

5.7.1 Strain rate field in the Indian Ocean and the Andaman Sea

For this study we assume a geometry of the IN–AU–Capricorn (CP) plate boundary zone similar to Royer & Gordon (1997), comprising the Chagos Ridge, Central Indian Basin, Ninetyeast Ridge, southern Bay of Bengal and Wharton Basin (Fig. 7a). The model strain rate

field (Fig. 7a) indicates ∼3 mm yr^{-1} of roughly N–S extension near the Chagos Ridge between the Capricorn and Indian plates. In the Central Indian Basin we see pure compression associated with ∼5 mm yr^{-1} of shortening and the compression direction rotates from NNE–SSW in the western part of the basin to more NNW–SSE in the eastern basin. In the northeastern Indian Ocean, comprising the southern Bay of Bengal, northern Ninetyeast Ridge, and Wharton Basin, the compression direction is NW–SE to NNW–SSE and the estimated relative motion between the Indian and Australian plates is ∼11 mm yr^{-1}. Our inferred AU–IN convergence rate of ∼11 mm yr^{-1} for the northeastern Indian Ocean is remarkably consistent with the total convergence of 125 ± 28 km since 11 Ma as was inferred by Royer & Gordon (1997) based on plate reconstructions in the Indian Ocean.

Our strain rate results are in general quite similar to expected extension and shortening directions discussed by Royer & Gordon (1997), and consistent with shortening directions inferred from seismic profiles (e.g. Bull & Scrutton 1992; Chamot-Rooke *et al.* 1993; Van Orman *et al.* 1995), and earthquake *P*–*T* axes (Fig. 7a). The consistency between the principal strain rate axes and earthquake focal mechanisms is partly imposed, because of the constraints from seismic moment tensors that are applied, *a priori*, to the style and direction of the model strain rate field. Tinnon *et al.* (1995) derived a seismic strain rate field from an inversion of earthquake focal mechanisms. Although Tinnon *et al.* (1995) used a different plate boundary geometry and did not define a Capricorn Plate, they obtained a solution quite similar in style and direction to our solution, with the exception of the Wharton Basin where Tinnon *et al.* (1995) predicted more N–S, instead of more NW–SE to NNW–SSE, shortening. The result presented here for the Wharton Basin is more consistent with observed NE–SW-trending undulations in the gravity field, which are thought to have resulted from NW–SE-directed compression (Weissel *et al.* 1980; McAdoo & Sandwell 1985; Haxby 1987). Also, the pure strike-slip earthquakes in the Wharton Basin and southern Ninetyeast Ridge region are consistent with the expected NW–SE compressional strain rates, indicating reactivation of N–S-trending fracture zones (Bull & Scrutton 1992; Deplus *et al.* 1998). The occurrence of the 2000 June 18, $M_W = 7.8$ strike-slip event in the Wharton Basin near Cocos Island (Robinson *et al.* 2001; Abercrombie *et al.* 2003) suggests that reactivation of old N–S fracture zones may occur as far east as 97°E in order to accommodate the NW–SE shortening between India and Australia.

We also present the model strain rate field for the Andaman Sea region (Fig. 7b). Our result resolves the partitioning of pure east–west compression along the Burma Trench and extension-dominated strain rates in the Andaman backarc. The predicted direction of extension, as it occurs along the spreading segments, is consistent with earthquake slip-vectors ∼N30°W). However, a significant component of right-lateral shear is also present and is in agreement with seismotectonics indicated by the focal mechanisms (Fig. 7b).

5.8 Arabia–Eurasia and Anatolia–Eurasia

The Arabian (AR) Plate motion is defined by a fit to the observed velocities at the GPSVEL station in Bahrain and station KIZI in southern Turkey, located about 100 km south of the Bitlis suture zone (McClusky *et al.* 2000). The model angular velocity describing AR–EU motion predicts 0.44°Myr^{-1} about a pole at 26.2°N and 20.4°E (Table 4), which is significantly different from the NUVEL-1A estimate. It is evident that the plate moves at a lower speed with respect to Eurasia than the NUVEL-1A predicted rate; we find an AR–EU velocity of 22.1 mm yr^{-1} at Bahrein, whereas NUVEL-1A predicts 30.5 mm yr^{-1}. This implies that AR–EU convergence at Bahrein is 27 per cent slower than the NUVEL-1A prediction.

We find an angular velocity vector describing Anatolia (AT)–EU relative motion (32.0°N, 33.4°E, 1.35°Myr^{-1}) that is, although at a somewhat higher rotation rate, insignificantly different from McClusky *et al.*'s (2000) estimate based on a similar set of GPS velocities. If all AT–EU relative motion is accommodated along the North Anatolian fault, slip rates can be inferred from the obtained AT–EU angular velocity. We find a slip rate for this fault of about 22–23 mm yr^{-1}, equal to the slip rate inferred by McClusky *et al.* (2000).

5.8.1 Strain rate field in the Aegean

The greater Aegean area is kinematically complex and seismically very active. In order to better understand the driving forces that are at the source of the tectonic complexity and to mitigate seismic hazard in the many populous areas in the region, a well-defined strain rate field is essential. Fig. 8(a) shows the principal axes of the model strain rate field for the Aegean area. The strain rate tensors are plotted as averages for each model grid area, indicating the true resolution of the global model. The strain rate field is similar to previous strain rate tensor calculations using similar sets of GPS velocities (Kahle *et al.* 1999, 2000), which are fitted very well by the model velocities (Fig. 8b). As discussed in detail by Kahle *et al.* (1999, 2000) many of the characteristics in the strain rate field solution are in good agreement with regional geology (e.g. grabens, troughs, and major strike-slip fault zones) and seismicity distribution (Fig. 8a).

5.9 Block motions in central and southeast Asia relative to Eurasia

It has been hypothesized that the northward motion of India with respect to Eurasia has caused the eastward extrusion of crustal material in east and southeast Asia (Molnar & Tapponnier 1975). Geological observations (e.g. Armijo *et al.* 1989; Peltzer *et al.* 1989; England & Molnar 1997) as well as modelling of earthquake moment tensors in central and east Asia (Holt *et al.* 1995) have confirmed the eastward motion of eastern Asia with respect to Eurasia. The model presented here, incorporating both Quaternary fault slip rates and geodetic velocities in the region, builds on the models presented by Holt *et al.* (2000a,b). Here, we present the motions of the Sunda, South China and Amurian blocks relative to Eurasia (Table 4, Fig. 9). The results for these blocks are a likely improvement over the results by Holt *et al.* (2000a), due to an improved model Eurasia reference frame and the inclusion of more GPS vectors.

The estimation of the Amurian (AM) block angular velocity is particularly difficult because of the expected low rate and because of the poor coverage of GPS sites on this block. For most GPS sites assumed to be on the Amurian block it is in fact arguable whether or not they are located on the stable portion of the block. In the current plate geometry seven GPS velocities are assumed to have been measured on the Amurian block, but they are taken from six different studies (Table 2). We find that the angular velocity vector that best describes AM–EU motion has a rotation pole at 58.8°N, 157.5°E at a rate of 0.03°Myr^{-1} (Table 4, Fig. 9). Although our result is subject to a large uncertainty (Fig. 9), the obtained angular velocity is close in pole location but 0.04°Myr^{-1} slower than the result by Holt *et al.* (2000a). Furthermore, our result is quite distinct from AM-angular velocities inferred from GPS vectors by Heki *et al.* (1999). The expected extension directions across the Baikal Rift are subparallel to the *T*-axes of normal fault earthquakes.

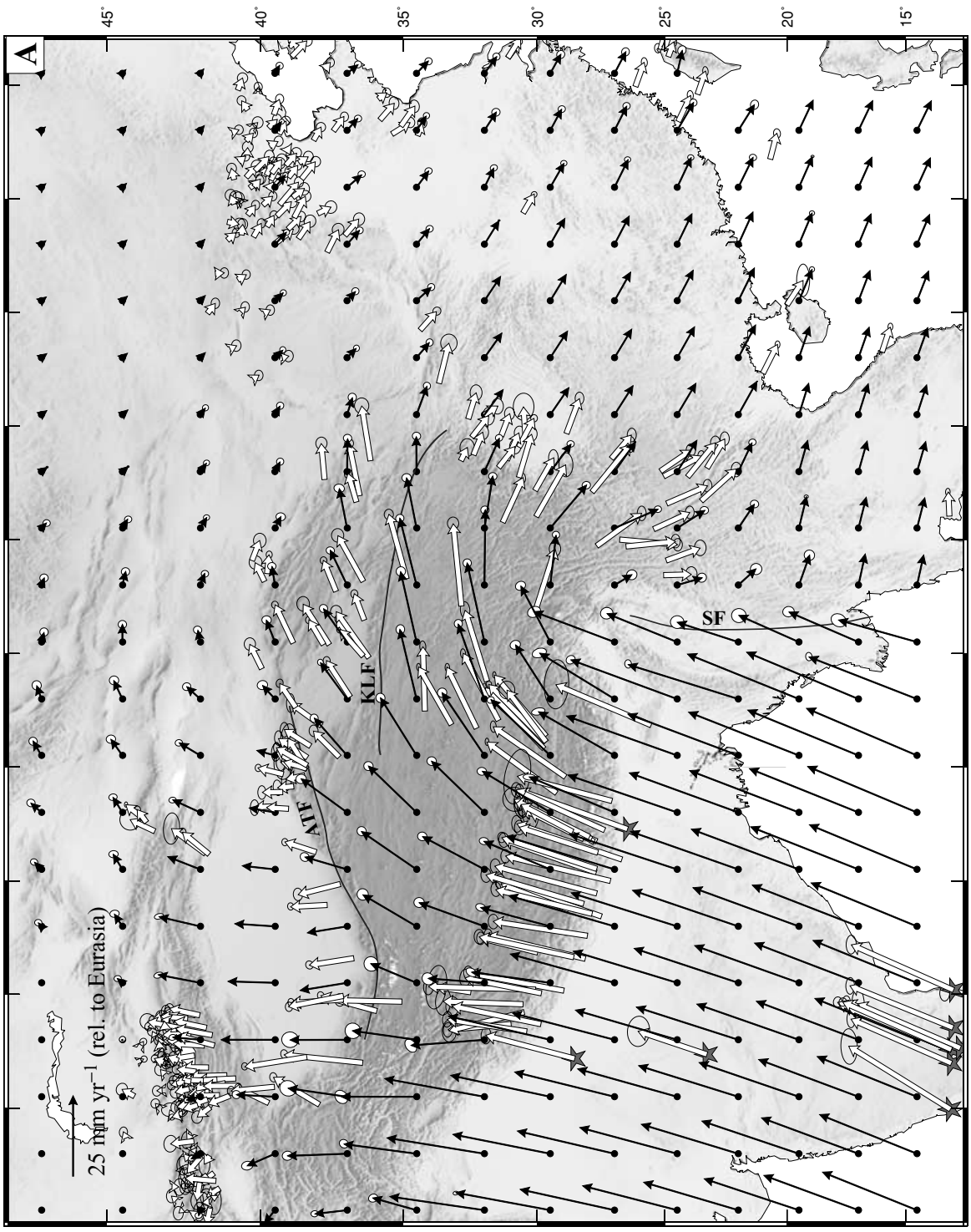

Figure 6. (a) Black vectors are model velocities at regularly spaced points in a model Eurasia reference frame. White vectors are geodetic velocities, after they have been rotated from their original reference frame into a model Eurasian reference frame, taken from several studies (Abdrakhmatov *et al.* 1996; Ma & Ryan 1998; Larson *et al.* 1999; Yu *et al.* 1999; Bendick *et al.* 2000; Shen *et al.* 2000; Chen *et al.* 2000; Paul *et al.* 2001; Michel *et al.* 2001; Shen *et al.* 2001; Wang *et al.* 2001, GPSVEL). Error ellipses represent 1σ uncertainty. Velocities at sites marked by a star are used to infer the angular velocity of the Indian Plate. For clarity some vectors in the Luzon–Taiwan region have been omitted. ATF, Altyn Tagh Fault; KLF, Kun Lun Fault; SF, Sagaing Fault. (b) Principal axes of the model (black arrows) and observed strain rates inferred from Quaternary fault slip rates (open arrows). Model strain rates are determined for $0.5^\circ \times 0.6^\circ$ areas, but they are shown here as averages for the outlined areas.

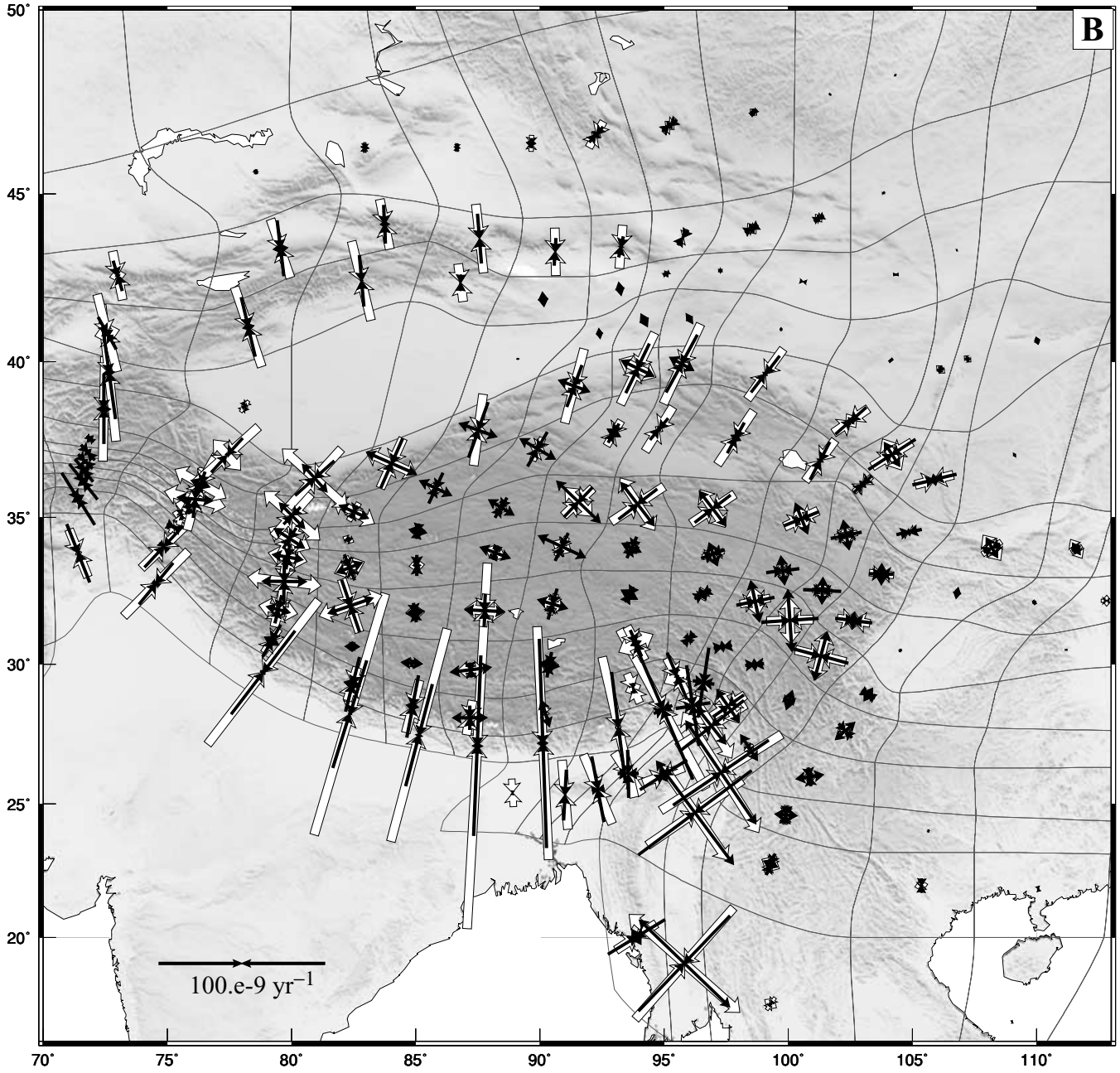

Figure 6. (*Continued*.)

Expected extension rates across the rift, on the other hand, do not exceed ∼2 mm yr^{-1}, which is lower than the ∼4.5 mm yr^{-1} from a regional GPS study (Calais *et al.* 1998) and also lower than the recently inferred 3.2 mm yr^{-1} Quaternary slip rate for the northern Baikal Rift (San'kov *et al.* 2000). We believe that a better constrained estimate of the Amurian Plate motion has to wait until more GPS measurements at more locations and over longer time-spans are available.

The angular velocity vector for South China (SC) with respect to Eurasia is subject to the assumed size and geometry of the South China Block. Owing to the presence of right-lateral faulting along the coast of South China and the occurrence of at least three earthquakes ($M_W = 5$) near Shanghai (Harvard CMT catalogue), we constrain the South China Block to be relatively small and bounded by the Longmen Shan in the west and the Qinling fault in the north. We assume that Wuhan and three other sites, measured by Chen *et al.* (2000), are located on this block. We find an SC–EU rotation rate of 0.22°Myr^{-1} about a pole at 47.3°N and 126.8°E, which yields an anticlockwise SC–EU motion (Fig. 9), consistent with results by Heki *et al.* (1999) and Holt *et al.* (2000a). On the southern part of the South China Block the predicted SC–EU motion amounts to 12 mm yr^{-1} in a direction roughly S66°E. We do not include Shanghai on the South China Block; whether or not Shanghai is part of the South China Block is reflected in a less than 1 mm yr^{-1} difference in model velocity in Shanghai. We estimate a model velocity of 6.5 ± 1.8 mm yr^{-1} at Shanghai in a direction of S59°E. Our obtained rate at Shanghai is consistent with the VLBI estimate by Molnar & Gipson (1996) and the GPS measurement by Chen *et al.* (2000), but

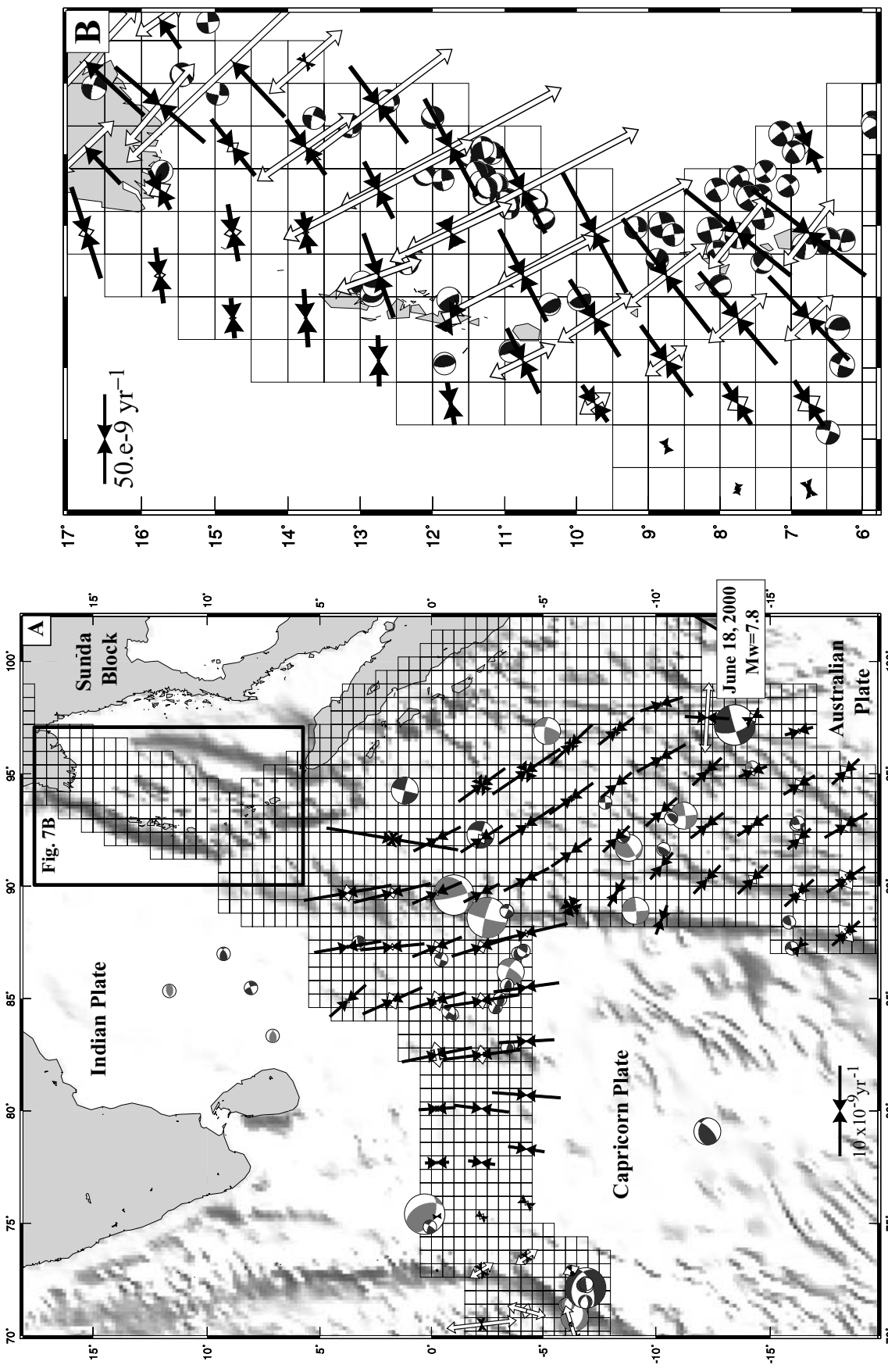

Figure 7. (a) Principal axes of the model strain rate field in the Indian Ocean, shown as roughly 2° × 2° averages (model strain rates are, however, calculated for each grid area shown). Black vectors indicate compression and open vectors indicate extension. Light shaded focal mechanisms are from events before 1977 from Tinnon *et al.* (1995) and dark shaded focal mechanisms are taken from the Harvard CMT catalogue. The latter focal mechanisms are used to set some *a priori* constraints on the style and direction (but not the magnitude) of the model strain rate field. For clarity strain rates axes and seismicity are omitted along the Sumatra Trench. The region shown in Fig. 7(b) is outlined by the box. (b) Principal axes of the model strain rate field in the Andaman Sea, shown for every other grid area. Black vectors indicate compression and open vectors indicate extension. Focal mechanisms are taken from the Harvard CMT catalogue and they have been used to set some *a priori* constraints on the style and direction (but not the magnitude) of the model strain rate field.

3.5–6 mm yr^{-1} lower than the VLBI estimate of Heki (1996) and GPS estimates of Kato *et al.* (1998), Heki *et al.* (1999) and Larson *et al.* (1999).

The notion that southeast Asia is moving with respect to Eurasia (Cardwell & Isacks 1978) has recently been confirmed by GPS measurements (Chamot-Rooke & Le Pichon 1999; Rangin *et al.* 1999; Simons *et al.* 1999; Michel *et al.* 2001). The independently moving entity has been named the Sundaland or Sunda (SU) block. Here we will use the latter name. In our model the motion of the Sunda block is inferred from eight GPS velocities from the GEODYSSEA project (Michel *et al.* 2001) and an additional velocity from the GPSVEL model in Singapore (NTUS). From the fit to the GPS velocities (Fig. 10) we find an SU–EU angular velocity with a rate of 0.13°Myr^{-1} about a pole at 26.0°N and 80.4°W (Table 4), which implies clockwise SU–EU motion (Fig. 9). This result is significantly different in location and rate from previous estimates based on regional modelling of earlier GEODYSSEA data (Chamot-Rooke & Le Pichon 1999; Kreemer *et al.* 2000b). From our model velocity field we find roughly 10 ± 1 mm yr^{-1} towards S78°E ± 9° along the northern margin of the Sunda block and about 6 ± 2 mm yr^{-1} towards S61°E ± 12° along the southern edge of the Sunda block (Fig. 10). The obtained ESE direction of the model velocities is consistent with the observed velocities after they have been rotated into a model Eurasia reference frame; at Tanjung on the southern part of the block the observed velocity is 7.0 mm yr^{-1} towards S78°E, and at Non Nuoc in the northern part of the block the rotated observed velocity is 11 mm yr^{-1} towards S72°E. Previous models of Sunda block motion predicted a motion in a roughly NE–E direction (Chamot-Rooke & Le Pichon 1999; Kreemer *et al.* 2000b). However, critical in the analysis of Sunda's motion with respect to Eurasia are the constraints placed on the motion of Sunda relative to South China for which the motion with respect to Eurasia is relatively well constrained. Any inferred Sunda–South China motion needs to be consistent with the lack of any significant deformation indicators between the two blocks (Fig. 10). Michel *et al.* (2001) found that velocities in northern and southern Sunda with respect to Eurasia equal 14 and 10 mm yr^{-1}, respectively. We find that an expected northern Sunda Block motion that exceeds ∼12 mm yr^{-1} (the inferred speed of the most southern edge of the South China Block with respect to Eurasia) would require left-lateral motion between the South China and Sunda blocks. Such left-lateral motion would be opposite in sense from the slip inferred from the few known earthquake slip vectors for events near the South China coast (Fig. 10) and is inconsistent with right-lateral motion of the Red River Fault (e.g. LeLoup *et al.* 1995). In the model presented here right-lateral motion is predicted on the southern end of the Red River fault at a rate of about 1–2 mm yr^{-1}, which we find to be insignificant. Unfortunately, the actual present-day slip rate on the Red River fault is still under debate (e.g. Zhao 1995; Cong & Feigl 1999).

5.10 Nubia—Somalia and Nubia—Eurasia

Whether or not the African Plate is comprised of two distinct entities (Nubia (NU) on the west and Somalia (SO) on the east) has been the source of much debate since the earliest plate model proposals (e.g. McKenzie *et al.* 1970; Chase 1972; Stein & Gordon 1984; Jestin *et al.* 1994; Chu & Gordon 1999). This question is of importance for the understanding of the relatively high seismicity occurrence in East Africa. In the case when Nubia and Somalia move separately a correlation is expected between relative plate motion and the seismotectonics in Eastern Africa. On the other hand, when Nubia and Somalia are kinematically one single entity then the East African Rift should be interpreted as a zone of intraplate deformation. The most recent studies that analysed plate motion data favour an independent Nubian and Somalian plate (Jestin *et al.* 1994; Chu & Gordon 1999). We know of only of two studies that directly measured the relative motion between Nubia and Somalia geodetically (Crétaux *et al.* 1998; Sella *et al.* 2002). Crétaux *et al.* (1998) inferred that the motions of the plates did not fit a single plate model, but they only used one station at the Somalian Plate (La Reunion). Sella *et al.* (2002) used the IGS stations of the Seychelles and near Malindi, Kenya, on the Somalian Plate and derived a pole for NU–SO relative motion near the southern extent of their mutual plate boundary zone. The extent of the plate boundary zone can be seen in Fig. 2 and is mainly determined from distributed seismicity occurrence using the Harvard CMT catalogue. In the study presented here we include two velocities at the Somalian Plate (the DORIS velocity at La Reunion and the GPSVEL estimate at Malindi) and eight stations on the Nubian Plate (Libreville, Arlit, Sainte-Hélène, Dakar (all from Crétaux *et al.* 1998), MATR (Egypt) (McClusky *et al.* 2000), and Mas Palomas, Gough Island and Sutherland (GPSVEL)). Stations at Djibouti and Hartebeestoek are considered to be situated in the NU–SO plate boundary zone. From this study we find that the motion between the Nubian and Somalian plates is not significant. We find an NU–SO model angular velocity of 0.03°Myr^{-1} of about 23.3°S and 21.9°E (Table 4). For most of the plate boundary the model predicts extension directions that are consistent with the *T*-axes of the majority of the focal mechanisms from the Harvard CMT catalogue. However, model velocities across the East African Rift do not exceed 1.6 mm yr^{-1} of extension. The anomalously low NU–SO relative motion is a surprising result, since it is much lower than any previous reported estimate of extension rate across the East African Rift (about 6 mm yr^{-1} is reported by Chu & Gordon 1999 and 5–7 mm yr^{-1} by Sella *et al.* 2002). It needs to be emphasized though that the uncertainty in our estimated pole location is very large, and we believe that the inclusion of more geodetic velocities in the future on both the Nubian and Somalian plates will place better constraints on this problem.

Of particular interest to the kinematics of the two 'African' plates is the observation that both plates move relatively slowly with respect to Eurasia, when compared with previous estimates (DeMets *et al.* 1994a; Larson *et al.* 1997). Our model predicts that NU–EU convergence amounts to about 4 ± 1 mm yr^{-1} near the Azores and 5–6 mm yr^{-1} in the eastern Mediterranean, whereas NUVEL-1A predicts convergence rates ranging from ∼6 to 10 mm yr^{-1} going from west to east along the Mediterranean Plate boundary. If NU–EU convergence is indeed as slow as suggested by the GPS measurements, it will have implications for both kinematic and dynamic models of the Mediterranean Plate boundary zone and, ultimately, for seismic hazard assessment for this region.

6 A NEW NO-NET-ROTATION MODEL

We have presented a global kinematic model for almost the entire Earth's surface. From an earlier version of this model Kreemer & Holt (2001) had determined a no-net-rotation reference frame and had calculated the angular velocities of most plates with respect to the NNR reference frame. Here we present a new NNR model that is a small revision from the model by Kreemer & Holt (2001). The small difference between this model and the recent model is twofold. First, the estimates of some relative angular velocities presented in this paper are small revisions of the model results on which Kreemer & Holt (2001) based their calculation. Secondly, in the model on

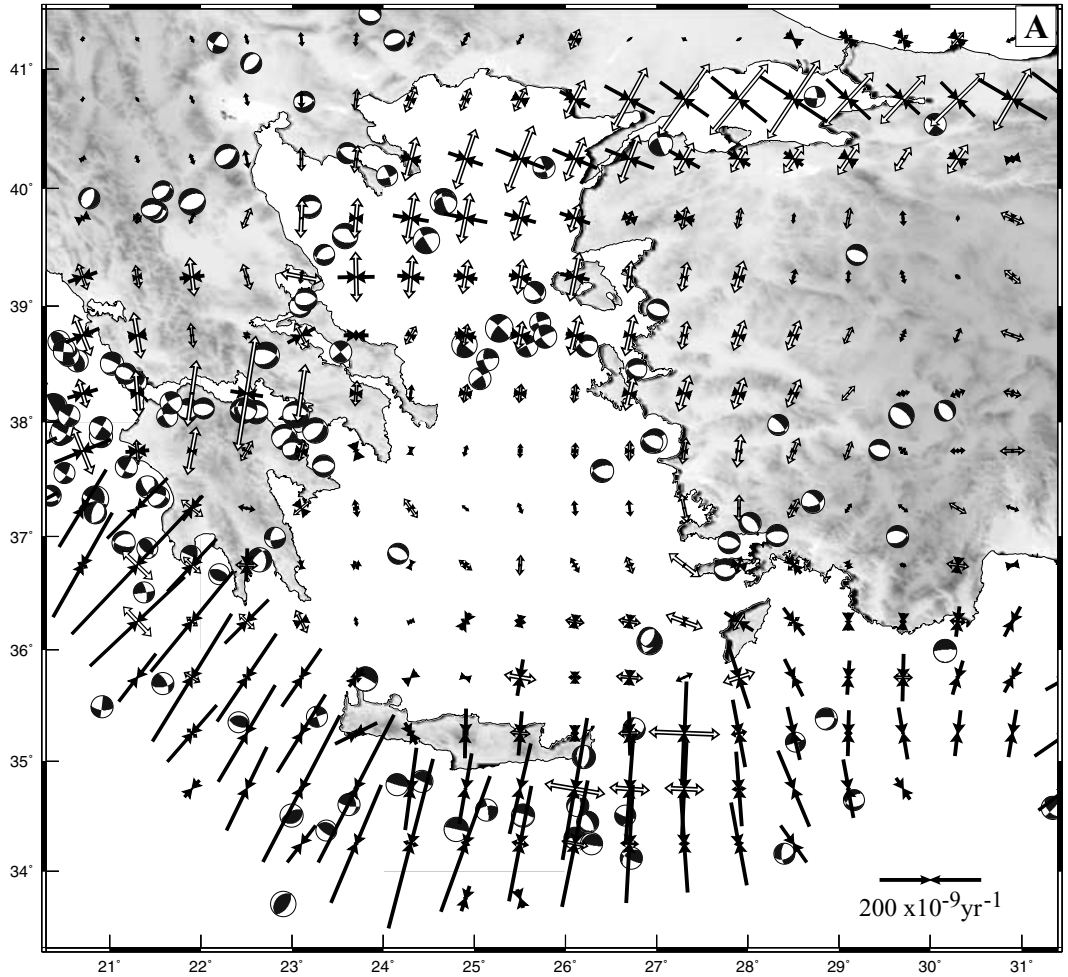

Figure 8. (a) Principal axes of the model strain rate field in the Aegean, shown as averages at the midpoints of each grid area in the model. Black vectors indicate compression and open vectors indicate extension. Focal mechanisms are taken from the Harvard CMT catalogue and they have been used to set some *a priori* constraints on the style and direction (but not the magnitude) of the model strain rate field. (b) Model (black vectors) and observed GPS vectors (white, McClusky *et al.* 2000; light grey, Cocard *et al.* 1999; dark grey, Clarke *et al.* 1998) within the Aegean. Error ellipses represent 1σ uncertainty and vectors are shown in our estimated Eurasian reference frame.

which Kreemer & Holt (2001) based their calculation they did not correct for the motions of the plates that are not constrained by geodetic velocities and which are otherwise likely to be erroneous (particularly in rate). Because the NNR model is based on the velocity field of the entire Earth's surface, it is important to add proper motions of the unconstrained plates to the model for the purpose of determining the NNR model. We have done this by adding the angular velocities of these plates in the calculation of the NNR reference frame. Unfortunately this means that we are adding angular velocities obtained from geological, seismic and seafloor data to the angular velocities derived geodetically in our model. However, this approach would lead to a closer estimate of the Earth's 'true' total velocity field in comparison with a case when we do not constrain the motions of the unconstrained plates at all. The angular velocities that we have applied are shown in Table 5. Table 6 shows the NNR angular velocities for all constrained plates (the reader is referred to Kreemer & Holt 2001, for a detailed explanation of the determination of the NNR model). Our new result indicates slightly faster plate motions than the model presented by Kreemer & Holt (2001); we find a total global root-mean-square velocity ($V_{\rm rms}$) (i.e. the minimum average velocity of the total Earth's surface) to be 38 mm yr^{-1}, whereas they found a $V_{\rm rms}$ of 37 mm yr^{-1}. However, for most plates the new angular rotations are not significantly different from the previous result. We find that the effect of including geologically derived angular velocities (in the NNR frame calculation) for the plates that are geodetically unconstrained increases the $V_{\rm rms}$ for most plates with a few tenths of one mm yr^{-1}. Similar to what Kreemer & Holt (2001) found, the NNR angular velocities presented here are at many places significantly different from the NNR model of Argus & Gordon (1991) (NNR-NUVEL-1A). In NNR-NUVEL-1A the surface of the Earth was assumed to be made up entirely of rigid plates. Regions of plate boundary deformation were defined to be part of rigid plates and the angular velocities were taken from the NUVEL1(A) model (DeMets *et al.* 1994a). We now know that the NUVEL-1A motion for several plates (e.g. Nazca, India, Arabia, Nubia) differs significantly from the geodetically determined present-day motion and that plate boundary zones often move at a significant speed compared with their adjacent plates. Kreemer & Holt (2001) found that the differences between present-day motions and NUVEL-1A motions is found to be the largest contributor to the different results between the new NNR model and NNR-NUVEL-1A, but the inclusion of plate boundary zones has in

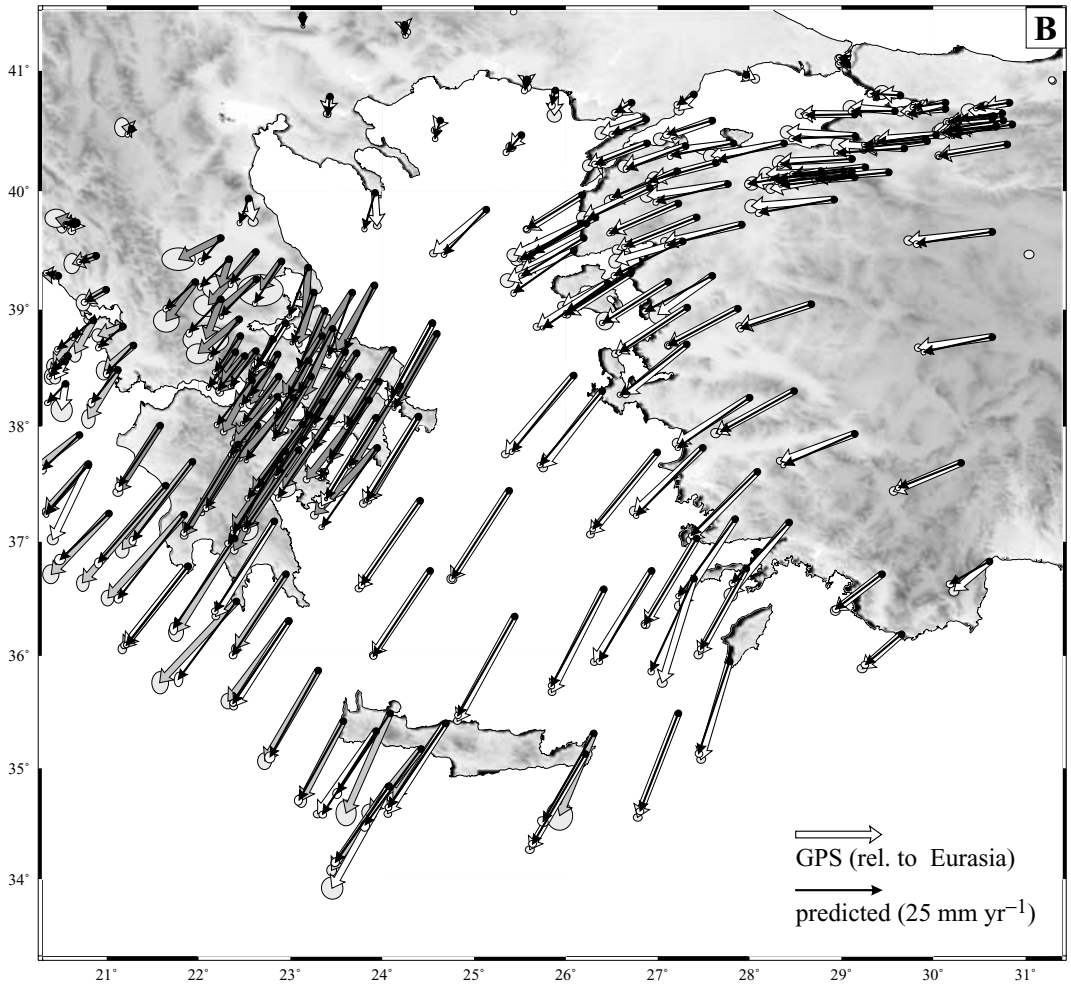

Figure 8. (*Continued*.)

some cases, e.g. Eurasia, a significant effect on the angular velocity as well.

7 DISCUSSION

Two of the key assumptions in the concept of plate tectonics are that plates are rigid and boundaries are narrow. While the model presented here incorporates diffuse deformation zones of considerable width, which is an improvement on previous plate motion models, the remainder of the Earth's surface is still assumed to behave rigidly. We obtain a good fit between the model and observed velocities on stable plates (Table 2) suggesting that, to first order, the assumption of plate rigidity is valid. Nevertheless, seismicity can be significant within the interiors of some plates (e.g. the Indian, Australian and North American plates) and, to the extent that intraplate seismicity is an expression of the same tectonic forces that govern seismicity within plate boundary zones, future models should ideally allow for intraplate strain rates to be accommodated as well. The current limitations to include intraplate strain rate calculations in the model presented here lie mainly within the relatively large uncertainties of geodetically measured velocities. Alternative estimates of intraplate strain rates could be obtained by dynamic models using force balance requirements (e.g. Wdowinski 1998; Bird & Liu 1999; Porth 2000). Also, Kreemer *et al.* (2002) speculated that perhaps the number of shallow earthquakes above a cut-off magnitude can be used to set bounds on intraplate strain rates. After initial findings by Kagan (1999, 2002) that there appears to be a strong global correlation between tectonic moment rate and the number of events above a cut-off magnitude along subduction zones, Kreemer *et al.* (2002) performed a more rigorous analysis using the strain rate model presented here. Kreemer *et al.* (2002) found that the global correlation found by Kagan (1999, 2002) appears to be applicable to both subduction zones and most regions of continental deformation. Based on their findings, Kreemer *et al.* (2002) argued that a correlation between seismicity rate and tectonic rate may also exist for intraplate settings. Whether this will prove to be correct or not, a combined knowledge of the regional strain rate and the seismicity rate could be very useful for all plate boundary zones to infer regional variations in seismic coupling, maximum moment and seismic hazard in general.

In the model presented here we have assumed that several smaller rigid blocks are present in the central and eastern Asia deformation zone; e.g. Amurian, Tarim, South China, Okhotsk and Sunda. The answer to the question of whether these blocks do in fact behave as independent rigid entities within a wide zone of distributed deformation has started to emerge more urgently with the use of GPS measurements. Although the relative angular velocities for these smaller blocks suffer in general from large uncertainties, the relatively good agreement between model and GPS velocities on these blocks (Table 2) suggests that, within the current uncertainties in

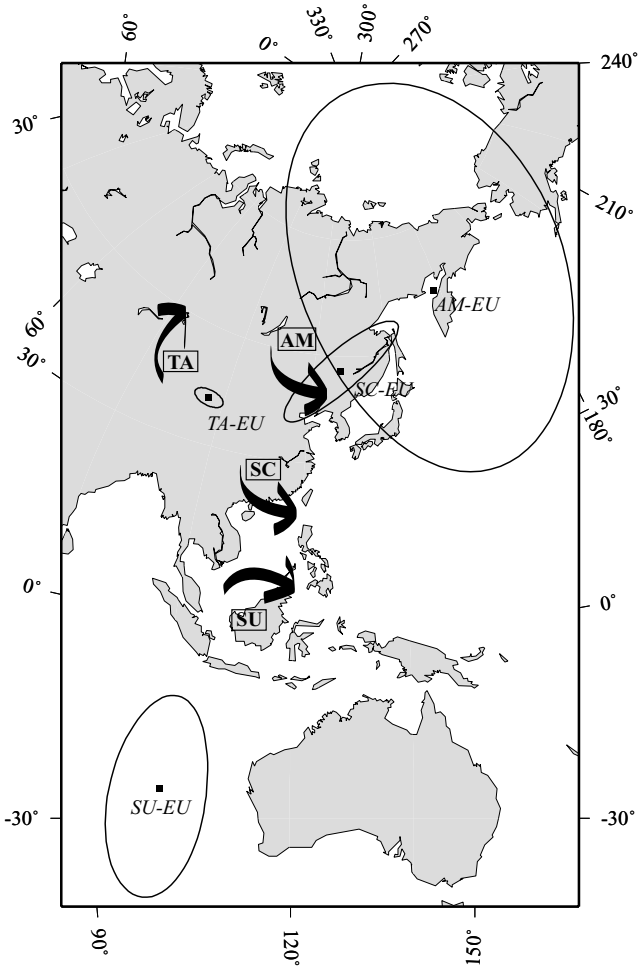

Figure 9. Euler poles and their 95 per cent confidence ellipses for the Amurian (AM), South China (SC), Sunda (SU), and Tarim (TA) Blocks with respect to Eurasia (EU). For each block the sense of rotation with respect to EU is indicated as well.

GPS velocities, rigidity of these blocks can be assumed. However, we would like to point out that due to both the small number of velocity measurements on some of these blocks and the occasionally low seismicity rates along their boundaries, the presented geometries of these blocks are subject to change. Therefore, to test the robustness of our results, we estimate the angular velocities for the Tarim, Amurian and South China blocks, with the assumption that these regions are low strain rate areas, instead of *a priori* constraining one single angular velocity to the areas comprising each block. For this test case we average the rotation vector function obtained for the deforming grid areas comprising each block. The angular velocities obtained in this way fall well within the uncertainties of the angular velocities for these blocks presented in Table 4, indicating that, given the uncertainty in our result, *a priori* rigidity can be assumed for these blocks. In another test we evaluate different models that assumed *a priori* rigidity the Tarim, Amurian and South China blocks but did not all have geodetic velocities on these blocks included. In this way we could (indirectly) investigate the effect of assuming different block geometries. We find, for instance, that the exclusion of the two sites in the Sea of Japan (believed to be on the rigid Amurian block) changed the AM–EU angular velocity only marginally. Similarly, we find that the exclusion of the velocities at Wuhan (located in the northeastern corner of the defined rigid South China Block) and at two sites located at the northern margin of the Tarim Basin (part of the assumed rigid Tarim block (TA)) does only slightly change the SC–EU and TA–EU angular velocities, respectively, with the result being within the 1σ uncertainty of the originally obtained angular velocities. These results indicate that the obtained angular velocities for the Amurian, South China and Tarim blocks are relatively robust (i.e. insignificantly different) with respect to chosen block geometries, and that an *a priori* assumption of rigidity of these blocks is appropriate.

For some of the plates and blocks the geometries are subject to uncertainty, and, because they do not contain geodetic measurements, their motions are ill-determined as well. Consequently, the validity of including proposed independent rigid blocks, such as the Caroline Plate (Weissel & Anderson 1978), cannot yet be tested. Similarly, it is also difficult to assess whether proposed entities such as the Gorda Block (Silver 1971) and Sinai subplate (McKenzie *et al.* 1970), which have not been included in the model, should be included as independent blocks.

To improve upon the kinematic model estimates for continental regions (in particular, for areas with low strain rates and few to no geodetic observations) additional geological information is welcomed. Currently we have only included Quaternary fault slip rates in central Asia. Concurrently, a large global catalogue of active, or potentially active faults is in the process of being compiled (Machette 2000). Such a data set may provide a tremendous amount of additional kinematic information that could be included in future modelling. Furthermore, the inclusion of regional centroid moment tensor data sets containing focal mechanisms with $5.5 \geq M \geq 4.5$ (e.g. Pondrelli *et al.* 2002; Braunmiller *et al.* 2002) will provide additional new constraints, particularly for low strain rate areas where moderate- and large-sized events are rare.

8 CONCLUSIONS

We have obtained a global strain rate field and velocity field in a joint fit to 3000 geodetic velocities and geological strain rates, inferred from Quaternary fault slip rates in Asia. Since fault slip rates are only included for central Asia, seismic moment tensors are used to *a priori* constrain the style and direction (but not magnitude) of the model strain rate field for all regions for which no fault slip rate estimates are included. By solving for the velocity gradient tensor field on almost the entire Earth's surface we have attempted to integrate the principle of rigid-body rotations of plates with the kinematics of plate boundary zones. We have shown strain rate field examples for central Asia, the Indian Ocean and the Aegean, all of which are consistent in style and distribution with existing regional information from geology and seismology (as well as gravity undulations in the Indian Ocean). We have also discussed inferred angular velocities for several plate pairs. We obtain significantly lower rotation rates for the motions of Nazca, Indian, Arabian and Nubian plates relative to Eurasia when compared with the NUVEL-1A model estimates, while a significantly higher rotation rate is found for the Caribbean Plate with respect to its adjacent plates. We find significant motions for the South China, Tarim and Sunda blocks with respect to Eurasia within a global kinematic model. On the other hand, no clearly distinct motion was observed between Nubia and Somalia. The model presented here has already made valuable contributions to the determination of a new present-day no-net-rotation model and has also been used to positively confirm the correlation between tectonic moment rate and the number of events above a cut-off magnitude along subduction zones and within most areas of continental deformation (Kreemer *et al.* 2002).

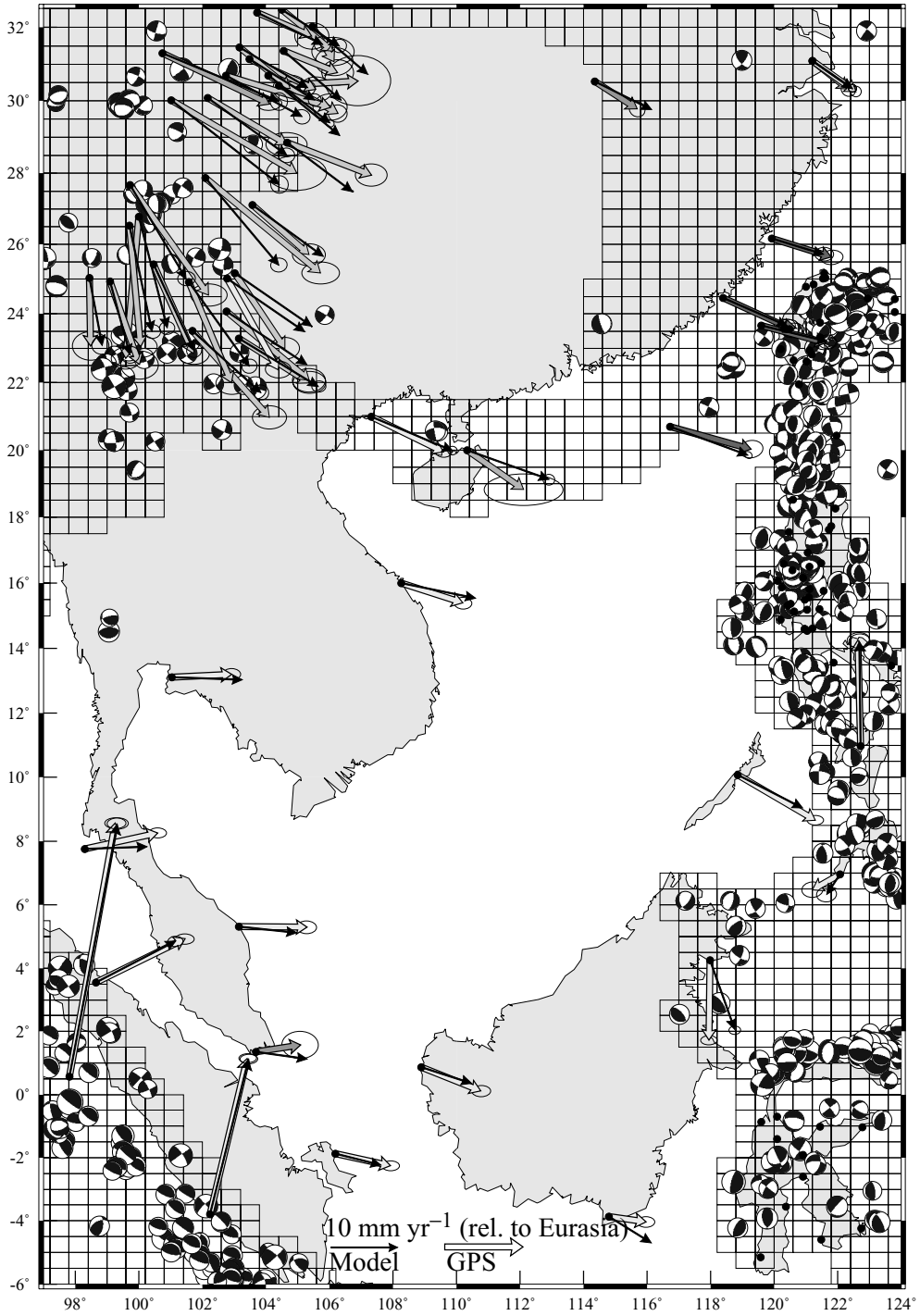

Figure 10. Model (black vectors) and geodetic velocities (grey vectors) in the South China–Sunda region. Velocities are with respect to a model Eurasia reference frame (i.e. geodetic velocities have been rotated from their original reference frame into the EU reference frame) and error ellipses represent 1σ uncertainty. Geodetic velocities have been taken from the following studies (each with their own grey shading): Ma & Ryan (1998), Yu *et al.* (1999), Shen *et al.* (2000), Chen *et al.* (2000), Michel *et al.* (2001), Shen *et al.* (2001), Wang *et al.* (2001), GPSVEL. For clarity most vectors in the Philippine–Taiwan region and in Sulawesi have been omitted. Also shown is the model grid and focal mechanisms for shallow events in the Harvard CMT catalogue.

ACKNOWLEDGMENTS

We thank J. Beavan, R. Bennett, E. Calais, J.-F. Crétaux, J. Freymueller, B. Hager, T. Kato, J. Kellogg and T. Sagiya for providing GPS vectors. We are grateful to W. Simons and the rest of the GEODYSSEA team for providing GPS vectors in southeast Asia. We wish to thank all members of the IGS community, and we are particularly grateful to G. Blewitt and D. Lavallée for making the GPSVEL version 0.2 model available. We wish to thank the USGS and SCEC communities for making their GPS solutions available. We thank J. Freymueller for a constructive review. We are grateful to L. Estey and C. Meertens at UNAVCO for setting up and maintaining an interactive website that displays the results of GSRM-1: http://www.world-strain-map.org. WEH is funded by NSF grants EAR-9909621 and

Table 5. Angular velocities of plates that are not constrained by geodetic velocities. These angular velocities are applied *a priori* in a version of the model used for the calculation of the no-net-rotation model. The Capricorn plate has been left unconstrained.

Plate	Lat. (°N)	Long. (°E)	$\dot{\omega}$ (°Myr^{-1})	Study
Caroline	−13.0	−36.0	0.70	Weissel & Anderson (1978)
Cocos	38.2	−109.6	2.00	DeMets (2001)
Juan de Fuca	5.7	32.1	0.58	Wilson (1993)
Rivera	26.0	−105.0	4.93	DeMets & Wilson (1997)
Scotia	50.9	−84.2	0.656	Pelayo & Wiens (1989)

Angular velocities are with respect to the Pacific Plate, where we have added the original published angular velocities of these plates with our geodetically derived angular velocities to determine the angular velocities of these plates with respect to the Pacific Plate.

Table 6. No-net-rotation angular velocity, 1σ error ellipse, $V_{\rm rms}$.

	NNR Euler vector			1σ error ellipse				
Plate	Lat. (°N)	Long. (°E)	$\dot{\omega}$ (°Myr^{-1})	$\sigma_{\rm max}$	$\sigma_{\rm min}$	$\zeta_{\rm max}$	σ_{ω}	$V_{\rm rms}$
Amurian	60.0	−103.8	0.302	1.3	0.5	−20	0.007	30.7
Anatolia	42.0	27.0	1.411	11.0	0.6	56	0.107	18.8
Antarctica	62.7	−120.6	0.242	0.5	0.5	−49	0.008	14.8
Arabia	50.6	−2.7	0.550	3.4	0.6	35	0.007	44.6
Australia	34.2	35.8	0.626	0.8	0.3	−52	0.004	61.8
Caribbean	37.0	−91.1	0.302	4.2	0.7	−26	0.029	15.5
Eurasia	56.4	−97.4	0.279	0.6	0.2	−81	0.005	25.3
India	52.6	−13.7	0.489	7.3	0.5	3	0.005	52.7
Nazca	44.4	−98.4	0.651	2.2	0.9	8	0.009	65.6
N. America	1.7	−82.3	0.211	0.4	0.3	−29	0.003	20.3
Nubia	52.6	−78.3	0.294	1.2	0.6	89	0.005	29.6
Okhotsk	−38.7	−43.9	1.037	12.0	1.2	−55	0.131	35.5
Pacific	−64.9	105.5	0.650	0.6	0.3	−86	0.003	64.1
Phil. Sea	−45.1	−28.9	0.874	14.6	2.7	−43	0.105	51.2
Somalia	57.3	−63.3	0.282	1.4	0.7	47	0.008	28.6
S. America	−14.5	−119.5	0.114	1.0	0.3	−43	0.004	11.8
S. China	73.8	−163.1	0.411	2.8	0.5	−20	0.011	41.0
Sunda	47.3	−90.2	0.392	1.9	0.5	−17	0.008	36.5
Tarim	−12.6	−86.8	0.641	3.7	0.7	6	0.032	33.5

1σ error ellipse axes are in degrees and $\zeta_{\rm max}$ is the azimuth of maximum axis in degrees; $V_{\rm rms}$, root-mean-square velocity (in mm yr^{-1}) relative to no-net-rotation frame. For 95 per cent confidence multiply standard errors with 2.45.

EAR-0001160, and NASA grant SENH99-0325-0015. WEH also thanks the International Lithosphere Programme for support of the Global Strain Rate Map Project, ILP II-8. Figures were prepared using GMT 3.0 (Wessel & Smith 1991).

REFERENCES

Abdrakhmatov, K.Ye. *et al.*, 1996. Relatively recent construction of the Tien Shan inferred from GPS measurements of present-day crustal deformation rates, *Nature,* **384,** 450–453.

Abercrombie, R.E., Antolik, M. & Ekström, G., 2003. The June 2000, M_w 7.9 earthquakes south of Sumatra: deformation in the India–Australia Plate, *J. geophys. Res.,* **108,** 10.1029/2001JB000 674.

Angermann, D., Klotz, J. & Reigber, C., 1999. Space-geodetic estimation of the Nazca–South America Euler vector, *Earth planet. Sci. Lett.,* **171,** 329–334.

Antonelis, K., Johnson, D.J., Miller, M.M & Palmer, R., 1999. GPS determination of current Pacific North America plate motion, *Geology,* **27,** 299–302.

Argus, D.F. & Gordon, R.G., 1990. Pacific–North American plate motion from very long baseline interferometry; Implications for the kinematics of the western United States, *J. geophys. Res.,* **95,** 17 315–17 324.

Argus, D.F. & Gordon, R.G., 1991. No-net-rotation model of current plate velocities incorporating plate motion model NUVEL-1, *Geophys. Res. Lett.,* **18,** 2039–2042.

Argus, D.F. & Gordon, R.G., 1996. Tests of the rigid-plate hypothesis and bounds on intraplate deformation using geodetic data from very long baseline interferometry, *J. geophys. Res.,* **101,** 13 555–13 572.

Argus, D.F. & Heflin, M., 1995. Plate motion and crustal deformation estimated with geodetic data from the Global Positioning System, *Geophys. Res. Lett.,* **22,** 1973–1976.

Armijo, R., Tapponnier, P. & Tonglin, H., 1989. Late Cenozoic right-lateral strike-slip faulting in southern Tibet, *J. geophys. Res.,* **94,** 2787–2838.

Avouac, J.P. & Tapponnier, P., 1993. Kinematic model of active deformation in central Asia, *Geophys. Res. Lett.,* **20,** 895–898.

Ball, M.M. & Harrison, C.G.A., 1970. Crustal plates in the central Atlantic, *Science,* **167,** 1128–1129.

Barazangi, M. & Isacks, B.L., 1976. Spatial distribution of earthquakes and subduction of the Nazca plate beneath South America, *Geology,* **4,** 686–692.

Beavan, J. & Haines, J., 2001. Contemporary horizontal velocity and strain rate fields of the Pacific–Australian plate boundary zone through New Zealand, *J. geophys. Res.,* **106,** 741–770.

Beavan, J. *et al.*, 1999. Crustal deformation during 1994–1998 due to oblique continental collision in the central Southern Alps, New Zealand, and

implications for seismic potential of the Alpine fault, *J. geophys. Res.,* **104,** 25 233–25 255.

Beavan, J., Silcock, D., Hamburger, M., Ramos, E., Thibault, C. & Feir, R., 2001. Geodetic constraints on postseismic deformation following the 1990 M_s 7.8 Luzon earthquake and implications for Luzon tectonics and Philippine Sea plate motion, *G3*, **2,** 2000GC000100.

Beavan, J., Tregoning, P., Bevis, M., Kato, T. & Meertens, C., 2002. The motion and rigidity of the Pacific plate and implications for plate boundary deformation, *J. geophys. Res.,* **107,** 10.029/2001JB000282.

Bendick, R., Bilham, R., Freymueller, J.T., Larson, K.M. & Yin, G.H., 2000. Geodetic evidence for a low slip rate in the Altyn Tagh fault system, *Nature,* **404,** 69–72.

Bennett, R.A., Davis, J.L. & Wernicke B.P., 1999. Present-day pattern of Cordilleran deformation in the western United States, *Geology,* **27,** 371–374.

Bergman, E.A., 1986. Intraplate earthquakes and the state of stress in oceanic lithosphere, *Tectonophysics,* **132,** 1–35.

Bergman, E.A. & Solomon, S.C., 1980. Oceanic intraplate earthquakes: implications for local and regional intraplate stress, *J. geophys. Res.,* **85,** 5389–5410.

Bevis, M. *et al.*, 1995. Geodetic observations of very rapid convergence and back-arc extension at the Tonga, *Nature,* **374,** 249–251.

Bevis, M., Kendrick, E.C., Smalley, R., Herring, T., Godoy, J. & Galban, F., 1999. Crustal motion north and south of the Arica deflection: comparing recent geodetic results from the central Andes, *G3*, **1,** 1999GC000011.

Bird, P. & Liu, Z., 1999. Global finite-element model makes a small contribution to intraplate seismic hazard estimation, *Bull. seism. Soc. Am.,* **89,** 1642–1647.

Biswas, N.N., Pujol, J., Tytgat, G. & Dean, K., 1986. Synthesis of seismicity studies for western Alaska, *Tectonophysics,* **131,** 369–392.

Braunmiller, J., Kradolfer, U., Bear, M. & Giardini, D., 2002. Regional moment tensor determination in the European-Mediterranean area—initial results, *Tectonophysics,* **356,** 5–22.

Bull, J.M. & Scrutton, R.A., 1992. Seismic reflection images of intraplate deformation, central Indian Ocean, and their tectonic significance, *J. geol. Soc. Lond.,* **149,** 955–966.

Calais, E. *et al.*, 1998. Crustal deformation in the Baikal rift from GPS measurements, *Geophys. Res. Lett.,* **25,** 4003–4006.

Cande, S.C., 1985. Nazca–South America plate interactions since 60 my B.P., in *Atlas of the Ocean Margin Program, Peru Continental Margin Region,* p. 14, eds Hussong, D.M., *et al.* Woods Hole, MA, Marine Science Institute.

Cande, S.C. & Leslie, R.B., 1986. Late Cenozoic tectonics of the southern Chile Trench, *J. geophys. Res.,* **91,** 471–496.

Cardwell, R.K. & Isacks, B.L., 1978. Geometry of the subducted lithosphere beneath the Banda Sea in eastern Indonesia from seismicity and fault plane solutions, *J. geophys. Res.,* **83,** 2825–2838.

Chamot-Rooke, N. & Le Pichon, X., 1999. GPS determined eastward Sundaland motion with respect to Eurasia confirmed by earthquakes slip vectors at Sunda and Philippine trenches, *Earth planet. Sci. Lett.,* **173,** 439–455.

Chamot-Rooke, N., Jestin, F., de Voogd, B. & Phèdre Working Group, 1993. Intraplate shortening in the central Indian Ocean determined from a 2100-km-long north–south deep seismic reflection profile, *Geology,* **21,** 1043–1046.

Chapman, M.E. & Solomon, S.C., 1976. North American–Eurasian plate boundary in northeast Asia, *J. geophys. Res.,* **81,** 921–930.

Chase, C.G., 1972. The, *n*-plate problem of plate tectonics, *Geophys. J. R. astr. Soc.,* **29,** 117–122.

Chen, Z. *et al.*, 2000. Global Positioning System measurements from eastern Tibet and their implications for India/Eurasia intercontinental deformation, *J. geophys. Res.,* **105,** 16 215–16 227.

Chu, D. & Gordon, R.G., 1999. Evidence for motion between Nubia and Somalia along the Southwest Indian ridge, *Nature,* **398,** 64–67.

Clarke, P.J. *et al.*, 1998. Crustal strain in central Greece from repeated GPS measurements in the interval 1989–1997, *Geophys. J. Int.* **135,** 195–214.

Cocard, M., Kahle, H.-G., Peter, Y., Geiger, A., Veis, G., Felekis, S., Paradissis, D. & Billiris, H., 1999. New constraints on the rapid crustal motion of the Aegean region: recent results inferred from GPS measurements (1993–1998) across the West Hellenic Arc, Greece, *Earth planet. Sci. Lett.,* **172,** 39–47.

Cong, D.C. & Feigl, K.L., 1999. Geodetic measurement of horizontal strain across the Red River fault near the Thac Ba, Vietnam, 1963–1994, *J. Geodesy,* **73,** 298–310.

Crétaux, J.-F., Soudarin, L., Cazenave, A. & Bouillé, F., 1998. Present-day tectonic plate motions and crustal deformations from the DORIS space system, *J. geophys. Res.,* **103,** 30 167–30 181.

Davies, P. & Blewitt, G., 2000. Methodology for global geodetic time series estimation: a new tool for geodynamics, *J. geophys. Res.,* **105,** 11 083–11 100.

DeMets, C., 1993. Earthquake slip vectors and estimates of present-day plate motions, *J. geophys. Res.,* **98,** 6703–6714.

DeMets, C., 2001. A new estimate for present-day Cocos-Caribbean plate motion: implications for slip along the Central American volcanic arc, *Geophys. Res. Lett.,* **28,** 4043–4046.

DeMets, C. & Dixon, T.H., 1999. New kinematic models for Pacific–North America motion from 3 Ma to present, I: Evidence for steady motion and biases in the NUVEL-1A model, *Geophys. Res. Lett.,* **26,** 1921–1924.

DeMets, C. & Wilson, D., 1997. Relative motions of the Pacific, Rivera, North American, and Cocos plates since 0.78 Ma, *J. geophys. Res.,* **102,** 2789–2806.

DeMets, C., Gordon, R.G., Stein, S. & Argus, D.F., 1987. A revised estimate of Pacific–North America motion and implications for western North America plate boundary zone tectonics, *Geophys. Res. Lett.,* **14,** 911–914.

DeMets, C., Gordon, R.G., Argus, D.F. & Stein, S., 1990. Current plate motions, *Geophys. J. Int.,* **101,** 425–478.

DeMets, C., Gordon, R.G., Argus, D.F. & Stein, S., 1994a. Effect of recent revisions of the geomagnetic reversal time scale on estimates of current plate motions, *Geophys. Res. Lett.,* **21,** 2191–2194.

DeMets, C., Gordon, R.G. & Vogt, P., 1994b. Location of the Africa–Australia–India Triple Junction and motion between the Australian and Indian plates: results from an aeromagnetic investigation of the Central Indian and Carlsberg Ridges, *Geophys. J. Int.* **119,** 893–930.

DeMets, C., Jansma, P.E., Mattioli, G.S., Dixon, T.H., Farina, F., Bilham, R., Calais, E. & Mann, P., 2000. GPS geodetic constraints on Caribbean–North America plate motion, *Geophys. Res. Lett.,* **27,** 437–440.

Deng, J. & Sykes, L.R., 1995. Determination of Euler pole for contemporary relative motion of Caribbean and North America plates using slip vectors of interplate earthquakes, *Tectonics,* **14,** 39–53.

Deplus, C. *et al.*, 1998. Direct evidence of active deformation in the eastern Indian oceanic plate, *Geology,* **26,** 131–134.

Dewey, J.F. & Bird, J.M., 1970. Mountain belts and the new global tectonics, *J. geophys. Res.,* **75,** 2625–2647.

Dixon, T.H. & Mao, A., 1997. A GPS estimate of relative motion between North and South America, *Geophys. Res. Lett.,* **24,** 535–538.

Dixon, T.H., Farina, F., DeMets, C., Jansma, P., Mann, P. & Calais, E., 1998. Relative motion between the Caribbean and North American plates and related boundary zone deformation from a decade of GPS observations, *J. geophys. Res.,* **103,** 15 157–15 182.

Dixon, T.H., Miller, M., Farina, F., Wang, H. & Johnson, D., 2000. Present-day motion of the Sierra Nevada block and some tectonic implications for the Basin and Range province, North American Cordillera, *Tectonics,* **19,** 1–24.

Drewes, H. & Angermann, D., 2001. The Actual Plate Kinematic and Crustal Deformation Model 2000 (APKIM 2000) as a Geodetic Reference System, *Proc. IAG Scientific Assembly*, Budapest.

Dziewonski, A.M., Chou, T.-A. & Woodhouse, J.H., 1981. Determination of earthquake source parameters from waveform data for studies of global and regional seismicity, *J. geophys. Res.,* **86,** 2825–2852.

Dziewonski, A.M., Ekström, G. & Maternovskaya, N.N., 2000. Centroid-moment tensor solutions for July–September, 1999. *Phys. Earth planet. Inter.,* **119,** 311–319.

Engdahl, E.R., van der Hilst, R. & Buland R., 1998. Global teleseismic relocation with improved travel times and procedures for depth determination, *Bull. seism. Soc. Am.,* **88,** 722–743.

England, P.C. & Houseman, G., 1986. Finite strain calculations of continental deformation, 2, Comparison with the India–Asia collision zone, *J. geophys. Res.,* **91,** 3664–3676.

England, P.C. & McKenzie, D.P., 1982. A thin viscous sheet model for continental deformation, *Geophys. J. R. astr. Soc.,* **70,** 295–321.

England, P.C. & Molnar, P., 1997. The field of crustal velocity in Asia calculated from Quaternary rates of slip on faults, *Geophys. J. Int.* **130,** 551–582.

Freymueller, J.T., Murray, M.H., Segall, P. & Castillo, D., 1999. Kinematics of the Pacific–North America plate boundary zone, northern California, *J. geophys. Res.,* **104,** 7419–7441.

Gan, W.J., Svarc, J.L., Savage, J.C. & Prescott, W.H., 2000. Strain accumulation across the Eastern California Shear Zone at latitude 36° 30′N, *J. geophys. Res.,* **105,** 16 229–16 236.

Giardini, D., 1999. The global seismic hazard assessment program (GSHAP)—1992/1999, *Ann. Geofis.,* **42,** 957–974.

Gordon, R.G., 1998. The plate tectonic approximation: plate nonrigidity, diffuse plate boundaries, and global plate reconstructions, *Ann. Rev. Earth Planet Sci.,* **26,** 615–642.

Gordon, R.G. & Stein, S., 1992. Global tectonics and space geodesy, *Science,* **256,** 333–342.

Gordon, R.G., DeMets, C. & Argus, D.F., 1990. Kinematic constraints on distributed lithospheric deformation in the equatorial Indian ocean from present motion between the Australian and Indian plates, *Tectonics,* **9,** 409–422.

Gordon, R.G., Argus, D.F. & Heflin, M.B., 1999. Revised estimate of the angular velocity of India relative to Eurasia, *EOS, Trans. Am. geophys. Un.,* **80,** Fall Meet. Suppl., F273.

Gutscher, M.A., Malavieille, J., Lallemand, S. & Collot, J.Y., 1999. Tectonic segmentation of the North Andean margin: impact of the Carnegie Ridge collision, *Earth planet. Sci. Lett.,* **168,** 255–270.

Haines, A.J. & Holt, W.E., 1993. A procedure for obtaining the complete horizontal motions within zones of distributed deformation from the inversion of strain rate data, *J. geophys. Res.,* **98,** 12 057–12 082.

Haines, A.J., Jackson, J.A., Holt, W.E. & Agnew, D.C., 1998. Representing distributed deformation by continuous velocity fields, *Science Report 98/5*, Institute of Geology and Nucl. Science, Wellington, New Zealand.

Haxby, W., 1987. *Gravity Field of the World's Oceans*, National Geophysical Data Center.

Heki, K., 1996. Horizontal and vertical crustal movements from three-dimensional very long baseline interferometry kinematic reference frame: implication for the reversal timescale revision, *J. geophys. Res.,* **101,** 3197–3198.

Heki, K. *et al.*, 1999. The Amurian plate motion and current plate kinematics in eastern Asia, *J. geophys. Res.,* **104,** 29 147–29 155.

Holt, W.E. & Haines, A.J., 1995. The kinematics of northern South Island New Zealand determined from geologic strain rates, *J. geophys. Res.,* **100,** 17 991–18 010.

Holt, W.E., Li, M. & Haines, A.J., 1995. Earthquake strain rates and instantaneous relative motion within central and east Asia, *Geophys. J. Int.,* **122,** 569–593.

Holt, W.E., Chamot-Rooke, N., Le Pichon, X., Haines, A.J., Shen-Tu, B. & Ren, J., 2000a. The velocity field in Asia inferred from Quaternary fault slip rates and GPS observations, *J. geophys. Res.,* **105,** 19 185–19 210.

Holt, W.E., Shen-Tu, B., Haines, A.J. & Jackson, J., 2000b. On the determination of self-consistent strain rate fields within zones of distributed continental deformation, in *The History and Dynamics of Global Plate Motions*, eds Richards, M.A., Gordon, R.G. & van der Hilst, R.D., AGU, Washington, DC.

Humphreys, E.D. & Weldon, R.J., 1994. Deformation across the western United States: a local estimate of Pacific–North America transform deformation, *J. geophys. Res.,* **99,** 19 975–20 010.

Isacks, B.L., Oliver, J. & Sykes, L.R., 1968. Seismology and the new global tectonics, *J. geophys. Res.,* **73,** 5855–5899.

Jackson, J., 2002. Faulting, flow, and the strength of the continental lithosphere, *Int. Geology Rev.,* **44,** 39–61.

Jansma, P., Mattioli, G.S., Lopez, A., DeMets, C., Dixon, T.H., Mann, P. & Calais, E., 2000. Neotectonics of Puerto Rico and the Virgin Islands, northeastern Caribbean, from GPS geodesy, *Tectonics,* **19,** 1021–1037.

Jestin, F., Huchon, P. & Gaulier, J.M., 1994. The Somalia plate and the East African Rift System: present-day kinematics, *Geophys. J. Int.* **116,** 637–654.

Johnson, H.O. & Agnew, D.C., 1995. Monument motion and measurement of crustal velocities, *Geophys. Res. Lett.,* **22,** 2905–2908.

Kagan, Y.Y., 1999. Universality of the seismic moment–frequency relation, *Pure appl. Geophys.,* **155,** 537–573.

Kagan, Y.Y., 2002. Seismic moment distribution revisited: II. Moment conservation principle, *Geophys. J. Int.,* **149,** 731–754.

Kahle, H.-G. *et al.*, 1999. The GPS strain rate field in the Aegean Sea and western Anatolia, *Geophys. Res. Lett.,* **26,** 2513–2516.

Kahle, H.-G., Cocard, M., Peter, Y., Geiger, A., Reilinger, R., Barka, A. & Veis, G., 2000. GPS-derived strain rate field within the boundary zones of the Eurasian, African, and Arabian plates, *J. geophys. Res.,* **105,** 23 353–23 370.

Kato, T. *et al.*, 1998. Initial results from WING, the continuous GPS network in the western Pacific area, *Geophys. Res. Lett.,* **25,** 369–372.

Kelleher, J. & McCann, W., 1976. Buoyant zones, great earthquakes, and unstable boundaries of subduction, *J. geophys. Res.,* **81,** 4885–4896.

Kogan, M.G. *et al.*, 2000. Geodetic constraints on the rigidity and relative motion of Eurasia and North America, *Geophys. Res. Lett.,* **27,** 2041–2044.

Kostrov, V.V., 1974. Seismic moment and energy of earthquakes, and seismic flow of rocks, *Izv. Acad. Sci. USSR Phys. Solid Earth, Engl. Transl.,* **1,** 23–44.

Kotzev, V., Nakov, R., Burchfiel, B.C., King, R. & Reilinger, R., 2001. GPS study of active tectonics in Bulgaria: results from 1996 to 1998. *J. Geodyn.,* **31,** 189–200.

Kreemer, C. & Holt, W.E., 2001. A no-net-rotation model of present-day surface motions, *Geophys. Res. Lett.,* **28,** 4407–4410.

Kreemer, C., Haines, A.J., Holt, W.E., Blewitt, G. & Lavallée, D., 2000a. On the determination of a global strain rate model, *Earth Planets Space,* **52,** 765–770.

Kreemer, C., Holt, W.E., Goes, S. & Govers, R., 2000b. Active deformation in eastern Indonesia and the Philippines from GPS and seismicity data, *J. geophys. Res.,* **105,** 663–680.

Kreemer, C., Holt, W.E. & Haines, A.J., 2002. The global moment rate distribution within plate boundary zones, in *Plate Boundary Zones*, Vol. 30, eds Stein S. & Freymueller, J.T.,Geodyn. Ser., 10/1029/030GD10. AGU, Washington, DC.

Lamb, S.H., 1994. Behaviour of the brittle crust in wide plate boundary zones, *J. geophys. Res.,* **99,** 4457–4483.

Larson, K.M., Freymueller, J.T. & Philipsen S., 1997. Global plate velocities from the Global Positioning System, *J. geophys. Res.,* **102,** 9961–9981.

Larson, K.M., Bürgmann, R., Bilham, R. & Freymueller, J.T., 1999. Kinematics of the India–Eurasia collision zone from GPS measurements, *J. geophys. Res.,* **104,** 1077–1093.

Lavallée, D. *et al.*, 2001. GPSVEL Project: towards a dense global GPS velocity field, *Proc. IAG Scientific Assembly*, Budapest.

LeLoup, P.H. *et al.*, 1995. The Ailao Shan-Red River shear zone (Yunnan, China), Tertiary transform boundary of Indochina, *Tectonophysics,* **251,** 3–84.

Leroy, S. & Mauffret, A., 1996. Intraplate deformation in the Caribbean region, *J. Geodyn.,* **21,** 113–122.

Ma, C. & Ryan, J.W., 1998. NASA Space Geodesy Program—GSFC DATA Analysis-1998, VLBI Geodetic Results 1979–1998, August.

Machette, M.N., 2000. Active, capable, and potentially active faults—a paleoseismic perspective, *J. Geodyn.,* **29,** 387–392.

MacMillan, D.S. & Ma, C., 1999. VLBI measurements of Caribbean and South American motion, *Geophys. Res. Lett.,* **26,** 919–922.

Mackey, K.G., Fujita, K., Gunbina, L.V., Kovalev, V.N., Imaev, V.S., Koz'min, B.M. & Imaeva, L.P., 1997. Seismicity of the Bering Strait region: evidence for a Bering block, *Geology,* **25,** 979–982.

Mao, A.L., Harrison, C.G.A. & Dixon, T.H., 1999. Noise in GPS coordinate time series, *J. geophys. Res.,* **104,** 2797–2816.

McAdoo, D.C. & Sandwell, D.T., 1985. Folding of the oceanic lithosphere, *J. geophys. Res.,* **90,** 8563–8569.

McCaffrey, R., Long, M.D., Goldfinger, C., Zwick, P.C., Nabelek, J.L., Johnson, C.K. & Smith, C., 2000. Rotation and plate locking at the southern Cascadia subduction zone, *Geophys. Res. Lett.,* **27,** 3117–3120.

McClusky, S. *et al.*, 2000. Global Positioning System constraints on plate kinematics and dynamics in the eastern Mediterranean and Caucasus, *J. geophys. Res.,* **105,** 5695–5719.

McKenzie, D.P., Davies, D. & Molnar, P., 1970. Plate tectonics of the Red Sea and East Africa, *Nature,* **226,** 243–248.

Michel, G. *et al.*, 2001. Crustal motion and block behaviour in SE-Asia from GPS measurements, *Earth planet. Sci. Lett.,* **187,** 239–244.

Miller, M.M., Johnson, D.J., Rubin, C.M., Dragert, H., Wang, K., Qamar, A. & Goldfinger, C., 2001. GPS-determination of along-strike variation in Cascadia margin kinematics: Implications for relative plate motion, subduction zone coupling, and permanent deformation, *Tectonics,* **20,** 161–176.

Minster, J.B. & Jordan, T.H., 1978. Present-day plate motions, *J. geophys. Res.,* **83,** 5331–5354.

Minster, J.B. & Jordan, T.H., 1987. Vector constraints on western US deformation from space geodesy, neotectonics, and plate motions, *J. geophys. Res.,* **92,** 4798–4804.

Molnar, P., 1988. Continental tectonics in the aftermath of plate tectonics, *Nature,* **335,** 131–137.

Molnar, P. & Gipson, J.M., 1996. A bound on the rheology of continental lithosphere using very long baseline interferometry: the velocity of south China with respect to Eurasia, *J. geophys. Res.,* **101,** 545–553.

Molnar, P. & Tapponier, P., 1975. Cenozoic tectonics of Asia: Effects of a Continental Collision, *Science,* **189,** 419–425.

Molnar, P., Atwater, T., Mammerickx, J. & Smith, S.M., 1975. Magnetic anomalies, bathymetry, and the tectonic evolution of the South Pacific since the late Cretaceous, *Geophys. J. R. astr. Soc.,* **40,** 383–420.

Müller, R.D. & Smith, W.H.F., 1993. Deformation of the oceanic crust between the North American and South American plates, *J. geophys. Res.,* **98,** 8275–8291.

Norabuena, E., Leffler-Griffin, L., Mao, A., Dixon, T., Stein, S., Sacks, I.S., Ocala, L. & Ellis, M., 1998. Space geodetic constraints of Nazca–South America convergence across the central Andes, *Science,* **279,** 358–362.

Norabuena, E.O., Dixon, T.H., Stein, S. & Harrison, C.G.A., 1999. Decelerating Nazca–South America and Nazca–Pacific plate motions, *Geophys. Res. Lett.,* **26,** 3405–3408.

Pardo-Casas, F. & Molnar, P., 1987. Relative motion of the Nazca (Farallon) and South American plates since late Cretaceous time, *Tectonics,* **6,** 233–248.

Paul, J. *et al.*, 2001. The motion and active deformation of India, *Geophys. Res. Lett.,* **28,** 647–650.

Pelayo, A.M. & Wiens, D.A., 1989. Seismotectonics and relative plate motions in the Scotia Sea region, *J. geophys. Res.,* **94,** 7293–7320.

Peltzer, G. & Saucier, F., 1996. Present-day kinematics of Asia derived from geologic fault rates, *J. geophys. Res.,* **101,** 27 943–27 956.

Peltzer, G., Tapponnier, P. & Armijo, R., 1989. Magnitude of the Late Quaternary left-lateral displacements along the north edge of Tibet, *Science,* **246,** 1285–1289.

Peltzer, G., Crampe, F. & King, G., 1999. Evidence of nonlinear elasticity of the crust from the $M_W = 7.6$ Manyi (Tibet) earthquake, *Science,* **286,** 272–276.

Pérez, O.J., Bilham, R., Bendick, R., Velandia, J.R., Hernández, N., Moncayo, C., Hoyer, M. & Kozuch, M., 2001. Velocity field across the southern Caribbean plate boundary and estimates of Caribbean/South-American plate motion using GPS geodesy 1994–2000, *Geophys. Res. Lett.,* **28,** 2987–2990.

Peterson, M.D. & Wesnousky, S.G., 1994. Fault slip rates and earthquake histories for active faults in southern CA, *Bull. seism. Soc. Am.,* **84,** 1608–1649.

Peterson, M.D. *et al.*, 1996. Probabilistic seismic hazard assessment for the state of California, *Division of Mines and Geology, Open-file Report 96–08*, Sacramento, California.

Pilger, R.H., 1981. Plate reconstructions, aseismic ridges, and low-angle subduction beneath the Andes, *Geol. Soc. Am. Bull.,* **92,** 448–456.

Pondrelli, S., Morelli, A., Ekström, G., Mazza, S., Boschi, E. & Dziewonski, A.M., 2002. European-Mediterranean regional centroid-moment tensors: 1997–2000, *Phys. Earth planet. Inter.,* **130,** 71–101.

Porth, R., 2000. A strain-rate-dependent force model of lithospheric strength, *Geophys. J. Int.,* **141,** 647–660.

Puntodewo, S.S.O. *et al.*, 1994. GPS measurements of crustal deformation within the Pacific–Australia plate boundary zone in Irian Jaya, Indonesia, *Tectonophysics,* **237,** 141–153.

Ramos, V.A. & Kay, S.M., 1992. Southern Patagonian plateau basalts and deformation: backarc testimony of ridge collisions, *Tectonophysics,* **205,** 261–282.

Rangin, C., Le Pichon, X., Mazzotti, S., Pubellier, M., Chamot-Rooke, N., Aurellio, M., Walpersdorf, A. & Quebral, R., 1999. Plate convergence measured by GPS across the Sundaland/Philippine Sea plate deformed boundary: the Philippines and eastern Indonesia, *Geophys. J. Int.,* **139,** 296–316.

Robinson, D.P., Henry, C., Das, S. & Woodhouse, J.H., 2001. Simultaneous rupture along two conjugate planes of the Wharton Basin earthquake, *Science,* **292,** 1145–1148.

Roest, W.R. & Collette, B.J., 1986. The Fifteen Twenty Fracture Zone and the North American–South American plate boundary, *J. geol. Soc. Lond.,* **143,** 833–843.

Royer, J.-Y. & Chang, T., 1991. Evidence for relative motions between the Indian and Australian plates during the last 20 m.y. from plate reconstructions: Implications for the deformation of the Indo-Australian plate, *J. geophys. Res.,* **96,** 11 779–11 802.

Royer, J.-Y. & Gordon, R.G., 1997. The motion and boundary between the Capricorn and Australian plates, *Science,* **277,** 1268–1274.

Sagiya, T., Miyazaki, S. & Tada, T., 2000. Continuous GPS array and present-day crustal deformation of Japan, *Pure appl. Geophys.,* **157,** 2303–2322.

San'kov, V., Déverchère, J., Gaudemer, Y., Houdry, F. & Filippov, A., 2000. Geometry and rate of faulting in the North Baikal Rift, Siberia, *Tectonics,* **19,** 707–722.

Sauber, J., McClusky, S. & King, R., 1997. Relation of ongoing deformation rates to the subduction zone process in southern Alaska, *Geophys. Res. Lett.,* **24,** 2853–2856.

Sclater, J. & Franchateau, J., 1970. The implications of terrestrial heat flow observations on current tectonics and geochemical models of the crust and upper mantle of the Earth, *Geophys. J.,* **20,** 509–542.

Sella, G., Dixon, T.H. & Mao, A., 2002. REVEL: a model for recent plate velocities from space geodesy, *J. geophys. Res.,* **107,** 10.1029/2000JB000033.

Shen, Z.-K., Zhao, C., Yin, A., Li, Y., Jackson, D.D., Fang, P. & Dong, D., 2000. Contemporary crustal deformation in east Asia constrained by Global Positioning System measurements, *J. geophys. Res.,* **105,** 5721–5734.

Shen, Z.-K., Wang, M., Li, Y., Jackson, D.D., Yin, A., Dong, D. & Fang, P., 2001. Crustal deformation along the Altyn Tagh Fault system, western China, from GPS, *J. geophys. Res.,* **106,** 30 607–30 621.

Shen-Tu, B., Holt, W.E. & Haines, A.J., 1998. Contemporary kinematics of the western United States determined from earthquake moment tensors, very long baseline interferometry, and GPS observations, *J. geophys. Res.,* **103,** 18 087–18 117.

Shen-Tu, B., Holt, W.E. & Haines, A.J., 1999. The kinematics of the western United States estimated from Quaternary fault slip rates and recent geodetic data, *J. geophys. Res.,* **104,** 28 927–28 955.

Silver, E.A., 1971. Tectonics of the Mendocino Triple Junction, *Geol. Soc. Am. Bull.,* **82,** 2965–2978.

Simons, W.M.F. *et al.*, 1999. Observing plate motions in SE Asia: geodetic results of the GEODYSSEA project, *Geophys. Res. Lett.,* **26,** 2081–2084.

Smith, D.E. *et al.*, 1994. Contemporary global horizontal crustal motion, *Geophys. J. Int.,* **119,** 511–520.

Somoza, R., 1998. Updated Nazca (Farallon)–South America relative motions during the last 40 Myr, *J. south am. Earth Sci.,* **11,** 211–215.

Stauder, W., 1975. Subduction of the Nazca plate under Peru as evidenced by focal mechanisms and by seismicity, *J. geophys. Res.,* **80,** 1053–1064.

Stein, S., 1993. Space geodesy and plate motions, in, *Contributions of Space Geodesy to Geodynamics: Crustal Dynamics, Geodyn. Ser.*, Vol. 23, pp. 5–20, eds Smith, D.E. & Turcotte, D.L., AGU, Washington, DC.

Stein, S. & Gordon, R.G., 1984. Statistical tests of additional plate boundaries from plate motion inversions, *Earth planet. Sci. Lett.,* **69,** 401–412.

Stein, S., Engeln, J.F., Wiens, D.A., Fujita, K. & Speed, R.C., 1982. Subduction seismicity and tectonics in the Lesser Antilles Arc, *J. geophys. Res.,* **87,** 8642–8664.

Stevens, C. *et al.*, 1999. Rapid rotations about a vertical axis in a collisional setting revealed by the Palu fault, Sulawesi, Indonesia, *Geophys. Res. Lett.,* **26,** 2677–2680.

Stock, J. & Molnar, P., 1982. Uncertainties in the relative positions of the Australia, Antarctica. Lord Howe, and Pacific plates since the late Cretaceous, *J. geophys. Res.,* **87,** 4697–4714.

Sutherland, R., 1995. The Australia–Pacific boundary and Cenozoic plate motions in the SW Pacific: some constraints from Geosat data, *Tectonics,* **14,** 819–831.

Tapponnier, P., Peltzer, G., Le Dain, A.Y., Armijo, R. & Cobbold, P., 1982. Propagating extrusion tectonics in Asia: new insights from simple experiments with plasticine, *Geology,* **10,** 611–616.

Taylor, F.W. *et al.*, 1995. Geodetic measurements of convergence at the New Hebrides island arc indicate fragmentation caused by an impringing aseismic ridge, *Geology,* **23,** 1011–1014.

Thatcher, W., 1995. Microplate versus continuum descriptions of active deformation, *J. geophys. Res.,* **100,** 3885–3894.

Tinnon, M.J., Holt, W.E. & Haines, A.J., 1995. Velocity gradients in the northern Indian Ocean inferred from earthquake moment tensors and relative plate velocities, *J. geophys. Res.,* **100,** 24 315–24 329.

Tregoning, P. *et al.*, 1998a. Estimation of current plate motions in Papua New Guinea from Global Positioning System observations, *J. geophys. Res.,* **103,** 12 181–12 203.

Tregoning, P., Tan, F., Gilliland, J., McQueen, H. & Lambeck, K., 1998b. Present-day crustal motion in the Solomon Islands from GPS observations, *Geophys. Res. Lett.,* **25,** 3627–3630.

Tregoning, P., Jackson, R.J., McQueen, H., Lambeck, K., Stevens, C., Little, R.P., Curley, R. & Rosa, R., 1999. Motion of the South Bismarck plate, Papua New Guinea, *Geophys. Res. Lett.,* **26,** 3517–3520.

Trenkamp, R., Kellogg, J.N., Freymueller, J.T. & Mora, H.P., 2002. Wide plate margin deformation, southern Central America and northwestern South America, CASA GPS observations, *J. south am. Earth Sci*., **15,** 157–171.

Van Orman, J., Cochran, J.R., Weissel, J.K. & Jestin, F., 1995. Distribution of shortening between the Indian and Australian plates in the central Indian Ocean, *Earth planet. Sci. Lett.,* **133,** 35–46.

Vine, F.J. & Matthews, D.H., 1963. Magnetic anomalies over ocean ridges, *Nature,* **199,** 947–949.

Vogt, P.R., 1973. Subduction and aseismic ridges, *Nature,* **241,** 189–191.

Vogt, P.R., Lowrie, A., Bracey, D.R. & Hey, R.N., 1976. Subduction of aseismic oceanic ridges: effects on shape, seismicity and other characteristics of consuming plate boundaries, *Geol. Soc. Am. Spec. Pap.,* **172,** 59.

Von Huene, R., Corvalán, J., Flueh, E.R., Hinz, K., Korstgard, J., Ranero, C.R., Weinrebe, W. & the CONDOR Scientists, 1997. Tectonic control of the subducting Juan Fernández Ridge on the Andean margin near Valparaiso, Chile, *Tectonics,* **16,** 474–488.

Walpersdorf, A., Vigny, C., Ruegg, J.-C., Huchon, P., Asfaw, L.M. & Kirbash, S.A., 1999. 5 years of geodynamics of the Afar triple junction area, *J. Geodyn.,* **28,** 225–236.

Wang, Q. *et al.*, 2001. Present-day crustal deformation in China constrained by Global Positioning System measurements, *Science,* **294,** 574–577.

Ward, S.N., 1990. Pacific–North America plate motions: new results from very long baseline interferometry, *J. geophys. Res.,* **95,** 21 965–21 981.

Ward, S.N., 1994. A multidisciplinary approach to seismic hazard in southern California, *Bull. seism. Soc. Am.,* **84,** 1293–1309.

Wdowinski, S., 1998. A theory of intraplate tectonics, *J. geophys. Res.,* **103,** 5037–5059.

Weber, J.C. *et al.*, 2001. GPS estimate of relative motion between the Caribbean and South American plates, and geologic implications for Trinidad and Venezuela, *Geology,* **29,** 75–78.

Weissel, J.K. & Anderson, R.N., 1978. Is there a Caroline plate?, *Earth planet. Sci. Lett.,* **41,** 143–158.

Weissel, J.K., Hayes, D.E. & Herron, E.M., 1977. Plate tectonic synthesis: the displacements between Australia, New Zealand, and Antarctica since the Late Cretaceous, *Mar. Geol.,* **25,** 231–277.

Weissel, J.K., Anderson, R.N. & Geller, C.A., 1980. Deformation of the Indo-Australian plate, *Nature,* **287,** 284–291.

Wessel, P. & Smith, W.F., 1991. Free software helps map and display data, *EOS, Trans. Am. geophys. Un.,* **72,** 441.

Wiens, D.A. *et al.*, 1985. A diffuse plate boundary model for Indian–Ocean tectonics, *Geophys. Res. Lett.,* **12,** 429–432.

Wilson, D.S., 1993. Confidence intervals for motion and deformation of the Juan de Fuca plate, *J. geophys. Res.,* **98,** 16 053–16 071.

Wysession, M.E., Wilson, J., Bartkó, L. & Sakata, R., 1995. Intraplate seismicity in the Atlantic Ocean basin: A teleseismic catalog, *Bull. seism. Soc. Am.,* **85,** 755–774.

Yu, S.-B., Kuo, L.-C., Punongbayan, R.S. & Ramos, E.G., 1999. GPS observation of crustal deformation in the Taiwan–Luzon region, *Geophys. Res. Lett.,* **26,** 923–926.

Zhang, J., Bock, Y., Johnson, H., Fang, P., Williams, S., Genrich, J., Wdowinski, S. & Behr, J., 1997. Southern California Permanent GPS Geodetic array: error analysis of daily position estimates and site velocities, *J. geophys. Res.,* **102,** 18 035–18 055.

Zhao, S.R., 1995. Joint inversion of observed gravity and GPS base-line changes for the detection of the active fault segment at the Red river fault zone, *Geophys. J. Int.* **122,** 70–88.

Zumberge, J.F. & Liu, R., eds, 1995. Densification of the IERS Terrestrial Reference Frame through regional GPS networks, *IGS Workshop Proc.* Pasadena, CA, IAG/IUGG.